Schweizerischer Erdbebendienst
Service Sismologique Suisse
Servizio Sismico Svizzero
Swiss Seismological Service

ETH zürich

SITE CHARACTERIZATION REPORT

SKEK: Kerns (OW), Kirchgemeinde

Agostiny Marrios Lontsi, Manuel Hobiger, Donat Fäh

Last Modification: 11th June, 2021

Schweizerischer Erdbebendienst (SED)
Service Sismologique Suisse
Servizio Sismico Svizzero
Servizi da Terratrembels Svizzer

ETH Zürich
Sonneggstrasse 5
8092 Zürich
Schweiz
agostiny.lontsi@sed.ethz.ch

Contents

Summary

A passive seismic survey was conducted at the strong-motion station SKEK at Kerns (OW) to characterize the underlying subsurface. The geophysical site characterization aims at using ambient seismic vibration recordings to infer the shear-wave velocity profile around the installed seismological station.
The H/V and ellipticity measurements for the nearest station to SKEK (SKEK48) show three peaks at 0.7, 3.6 and 20.5 Hz with H/V amplitudes of 2.6, 9.1, and 2.4, respectively. The array methods used include high-resolution frequency-wavenumber, wavefield decomposition, interferometric multichannel analysis of surface waves, and spatial autocorrelation. They provide clear and broad phase velocity dispersion curves for Rayleigh and Love waves in the frequency range between 4.2 and 24.4 Hz. Two Rayleigh wave branches are observed within this frequency band and interpreted as fundamental and first higher modes. One Love wave branch is observed and interpreted as fundamental mode.
Two combined inversions are performed, one inverting the fundamental mode ellipticity and dispersion curves, and the second inverting the full H/V and dispersion curves. The resulting best velocity profiles indicate discontinuities at around 2 m depth and a velocity gradient between 30 and 75 m for the two inversions.
The average V_{S30} from the two inversions are 371 $\pm$ 4 m/s and 388 $\pm$ 3 for the first and second inversion, respectively. This V_{S30} value corresponds to ground type B in EC8 (European standard) and to ground type C in SIA261 (Swiss standard). The main difference from the inversions is in the velocity of the half-space below 100 m and has positive consequences on the interpretation of the observed empirical amplification functions.

1 Introduction

As part of the second phase of the Swiss Strong Motion Network renewal project, a strong motion station was built close to the Kirchgemeinde in Kerns (OW). The station replaces the old station SKEH that was located in Hobiel, about 450 m west of the new station location. SKEH was running from 1992 to 2012. The new station SKEK went operational on February 24th, 2019. At this site, a passive seismic survey was performed to record the propagating ambient noise wavefield. We use single station and array methods to analyze the characteristics of Rayleigh and Love waves in the recorded noise wavefields. In a first inversion, the estimated fundamental mode ellipticity branches and the phase velocity dispersion information are combined to infer the underlying subsurface structure and the corresponding 1D shear wave velocity profile. In a second inversion, the full H/V curve and the phase velocity dispersion information are used (Lontsi et al., 2016b).

2 Site and geological setting

Figure 1 shows the location of Kerns in Switzerland and the surface geology at the array sites. All stations sit on unconsolidated sediment deposits.

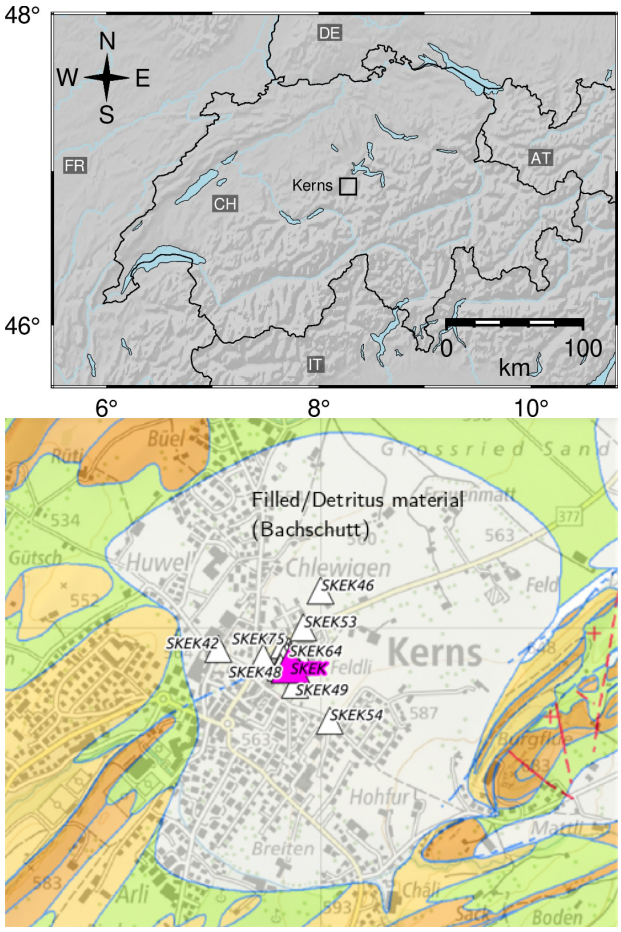

Figure 1: Top: Location of the strong motion station at Kerns (OW). Bottom: The strong motion station SKEK and the array geometry on top of the surface geology for the measurement site.

3 Overview of the site characterization measurement

In order to characterize the local underground structure around station SKEK, a passive seismic array measurement was carried out on October 8^{th}, 2020. Figure 2 shows an aerial image of the survey site, indicating the permanent station SKEK (purple triangle) and the temporary array deployment (white triangles) for ambient noise measurements. The array consisted of 16 stations. It was planned to have five rings of three stations each around a central station. The minimum and maximum inter-station distances of the final array layout were 5.79 and 349.55 m, respectively. The seismic stations consisted of Lennartz 3C 5 s sensors connected to Centaur digitizers. A total of 12 digitizers were used. Twelve sensors were connected to the A channels of the digitizers and another four sensors were connected to the B channels. The sampling rate was 200 Hz. The stations of the temporary array are named by adding a two-digit number to the permanent station name. The two-digit numbers are directly related to the last two digits of the recorder serial numbers for stations connected to channel A and augmented by 20 for stations connected to channel B. The array continuously recorded ambient vibrations for 3h between 10:50 and 13:50 (UTC).
The station locations have been measured by a differential GPS system (Leica Viva GS10) which was set up to measure with a precision better than 5 cm. This precision was achieved at all stations, with a maximum uncertainty of 3 cm.

Figure 2: Aerial image of the survey site at Kerns with the strong motion station location and array configuration. Source of the aerial map: Federal Office of Topography.

4 Single-station analysis

4.1 Microtremor H/V and ellipticity estimation

The microtremor H/V spectral ratio and the ellipticity curves are obtained using 6 different techniques:

- geopsyhv: full microtremor H/V estimation (www.geopsy.org);
- RayDec, optimized for Rayleigh wave ellipticity estimation (Hobiger et al., 2009);
- FTAN, optimized for Rayleigh wave ellipticity estimation (Fäh et al., 2009);
- CLASS, optimized for Rayleigh wave ellipticity estimation (Fäh et al., 2001);
- VPTFA, optimized for Rayleigh wave ellipticity estimation (Poggi & Fäh, 2010);
- MTSPEC, optimized for Rayleigh wave ellipticity estimation (Burjánek et al., 2010).

The H/V and Rayleigh wave ellipticity results for each station using the 6 techniques are shown in Figure 3 for comparison. The variability of the H/V spectral ratio within the array are highlighted by showing the H/V spectral ratio curves on the aerial map (Figure 4).
At each station, two peak frequencies are picked in the frequency range between 0.2 and 20.0 Hz (Figure 5).
Between 0.2 and 20 Hz, two peaks are observed at 0.7 and 3.6 Hz. The peak at 3.6 Hz is dominant. Most stations show one major frequency peak at a frequency between 2.9 Hz (SKEK45) and 6.3 Hz (SKEK46). The variations in the peak H/V frequency suggests that the subsurface sediment thickness is variable. The station SKEK46 that is located on the outer ring is particularly characterized by a broad peak frequency between 5 and 9 Hz. This can be related to the local structure at this particular station location. Above 20 Hz, some stations present an additional peak on the H/V spectral ratio curves around 20.5 Hz (see Figure 3).

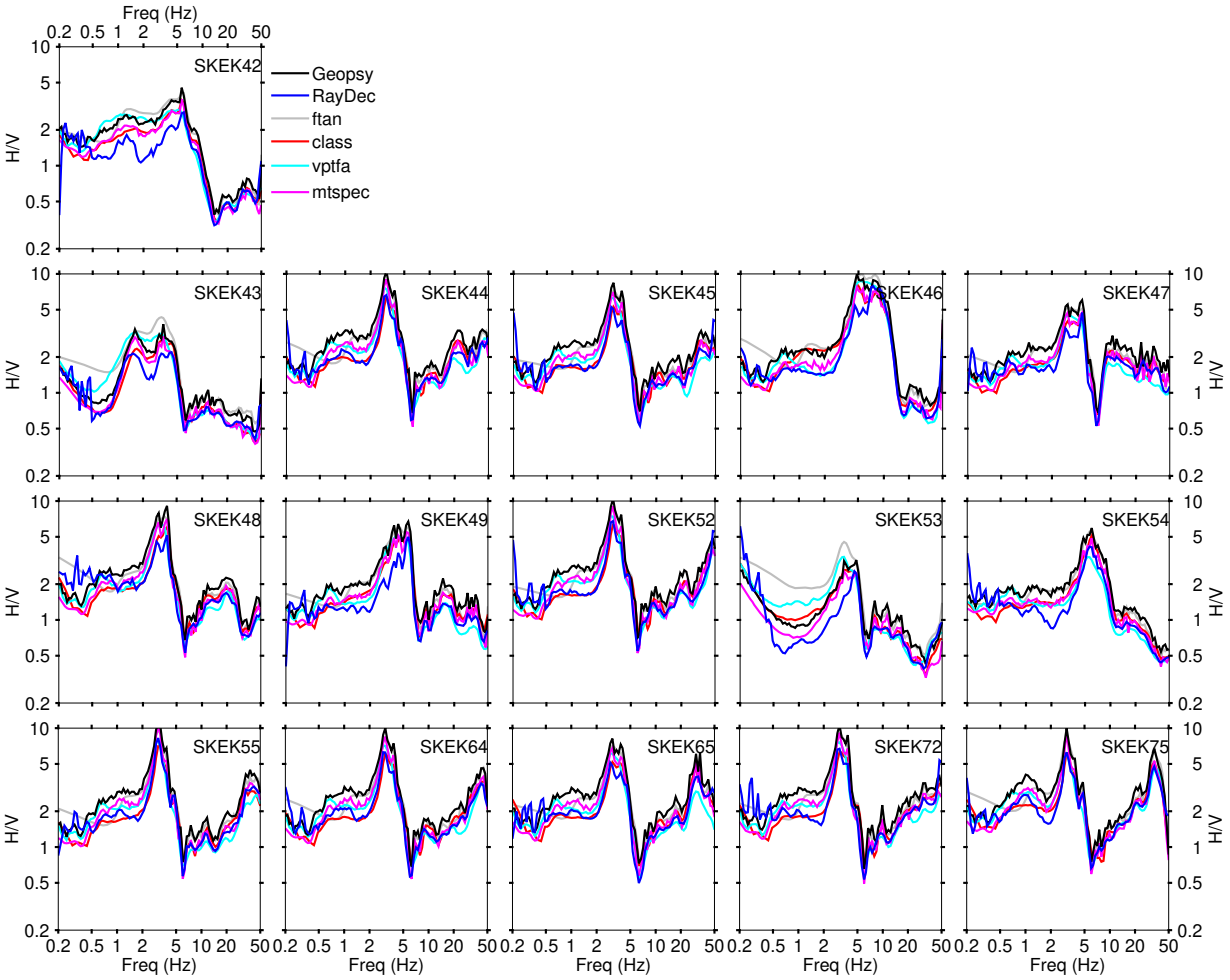

Figure 3: Ellipticity and H/V spectral ratio estimation using different techniques.

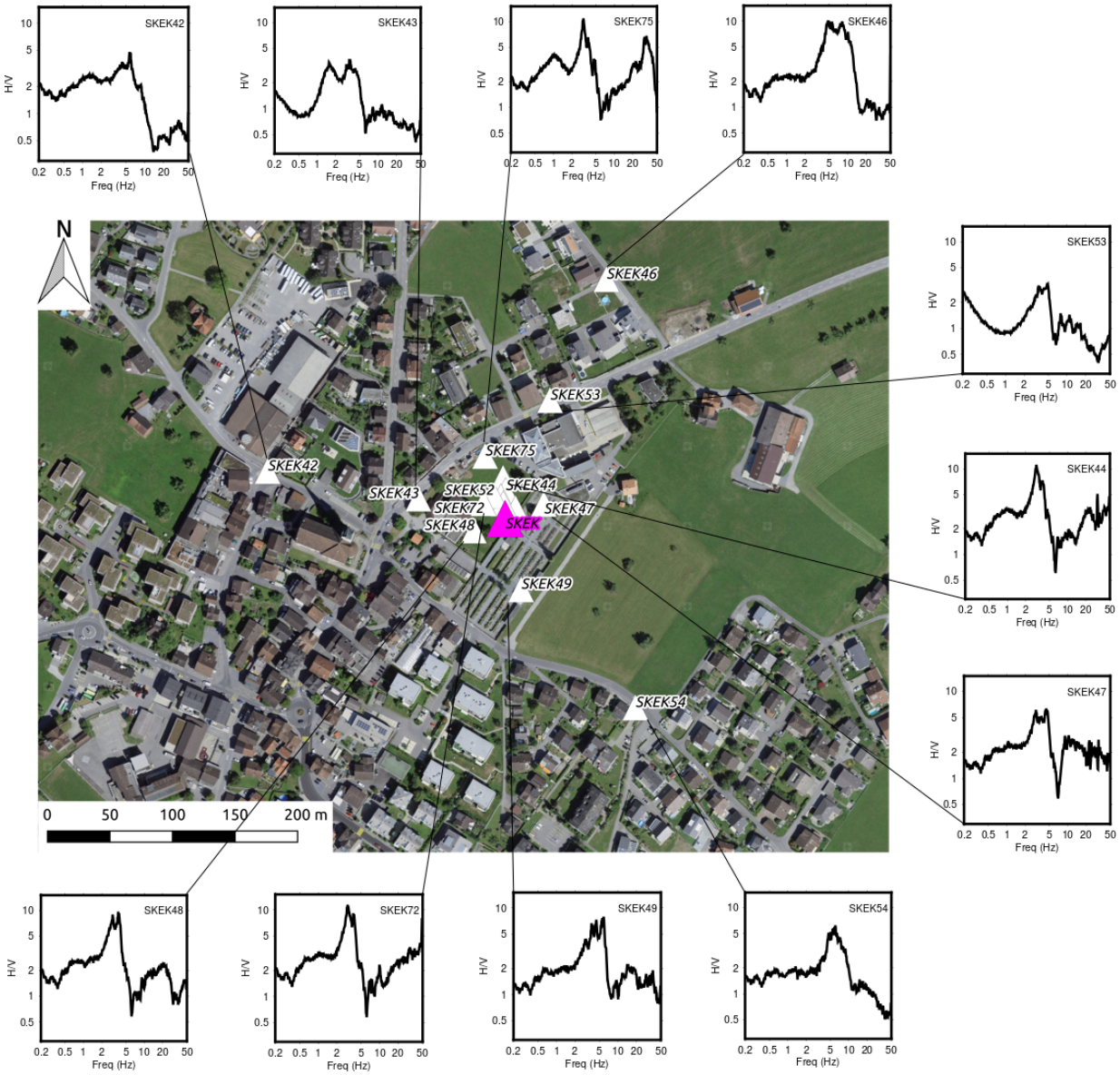

Figure 4: H/V spatial variability around the strong motion station at Kerns.

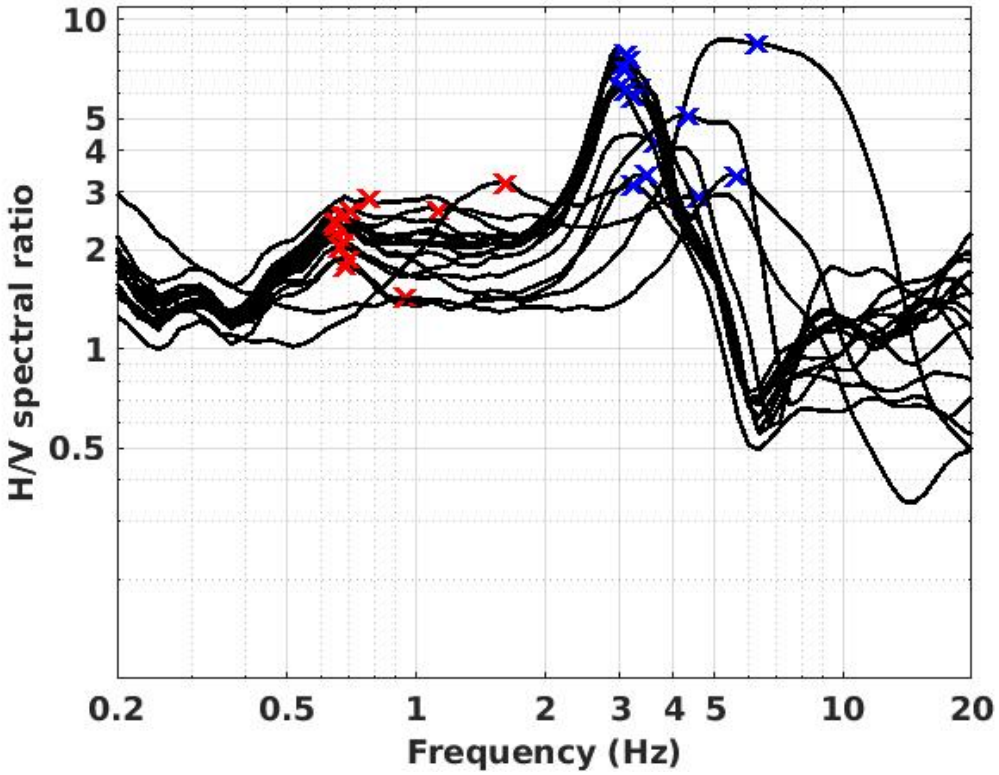

Figure 5: Overview of the H/V curves of the different stations, obtained using the ellipticity technique by Poggi & Fäh (2010); see also *vptfa* in Figure 3. For the presented frequency range (0.2 - 20 Hz), the red and blue markers indicate the frequencies of the first and second maxima in the H/V spectral ratio curves.

4.2 Polarization analysis

Following Burjánek et al. (2010, 2012), the polarization analysis is performed to assess potential 2D effects. The results are shown in Figure 6 for station SKEK48, the central station of the array.

The analysis indicates no preferential polarization except for a slight indication of polarized particle motion around 3 Hz, where the low ellipticity value indicates a predominantly linear particle motion. This is in agreement with the strong H/V and Rayleigh wave ellipticity values at this frequency. However, this linear polarization is not related with a predominant strike direction. Between 5 and 10 Hz, a predominant strike direction is observed, which is not related with linear particle motion. This angle correlates with the construction work ongoing near to the site and is not related to structural changes.

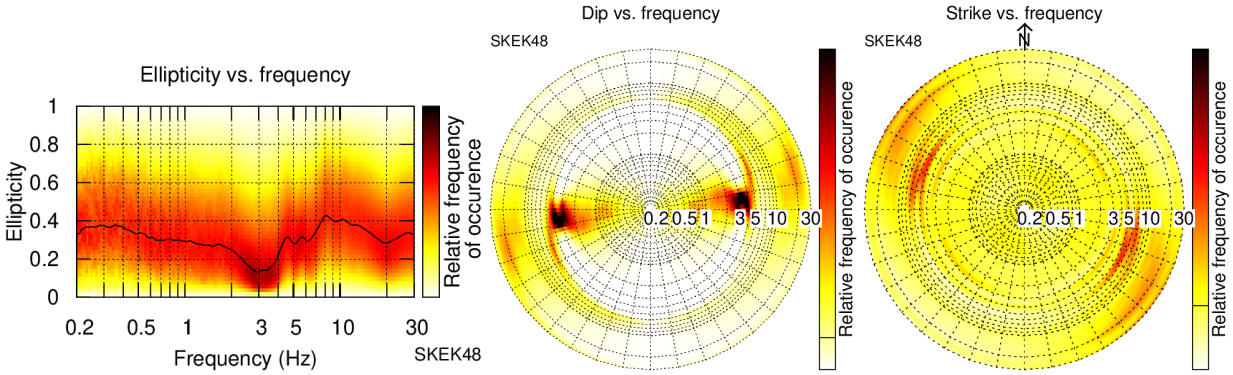

Figure 6: Polarization analysis for station SKEK48, located next to the permanent station.

5 Array analysis

The phase velocities for Rayleigh and Love waves are estimated for the full array of 16 stations using four different array methods:

1. Spatial autocorrelation (SPAC, Aki 1957; Bettig et al. 2001);
2. High resolution frequency-wavenumber (HRFK, Poggi & Fäh 2010);
3. Wavefield decomposition (WaveDec, Maranò et al. 2012);
4. Interferometric Multichannel Analysis of Surface Waves (IMASW, Lontsi et al. 2016a).

5.1 SPAC

The SPAC (Aki, 1957) curves of the vertical components have been calculated using the M-SPAC (Bettig et al., 2001) technique implemented in geopsy. Rings with different radius ranges had been defined and for all station pairs with distance inside this radius range, the cross-correlation was calculated over a wide frequency range. These cross-correlation curves are averaged for all station pairs of the respective ring and give the SPAC curves.
The SPAC rings are shown in Figure 7. The phase velocity is obtained through a non-linear inversion of the estimated autocorrelation coefficients. This was made with the function spac2disp of the geopsy package. Using SPAC, we can retrieve a Rayleigh wave phase-velocity dispersion curve between 4.48 and 6.34 Hz.

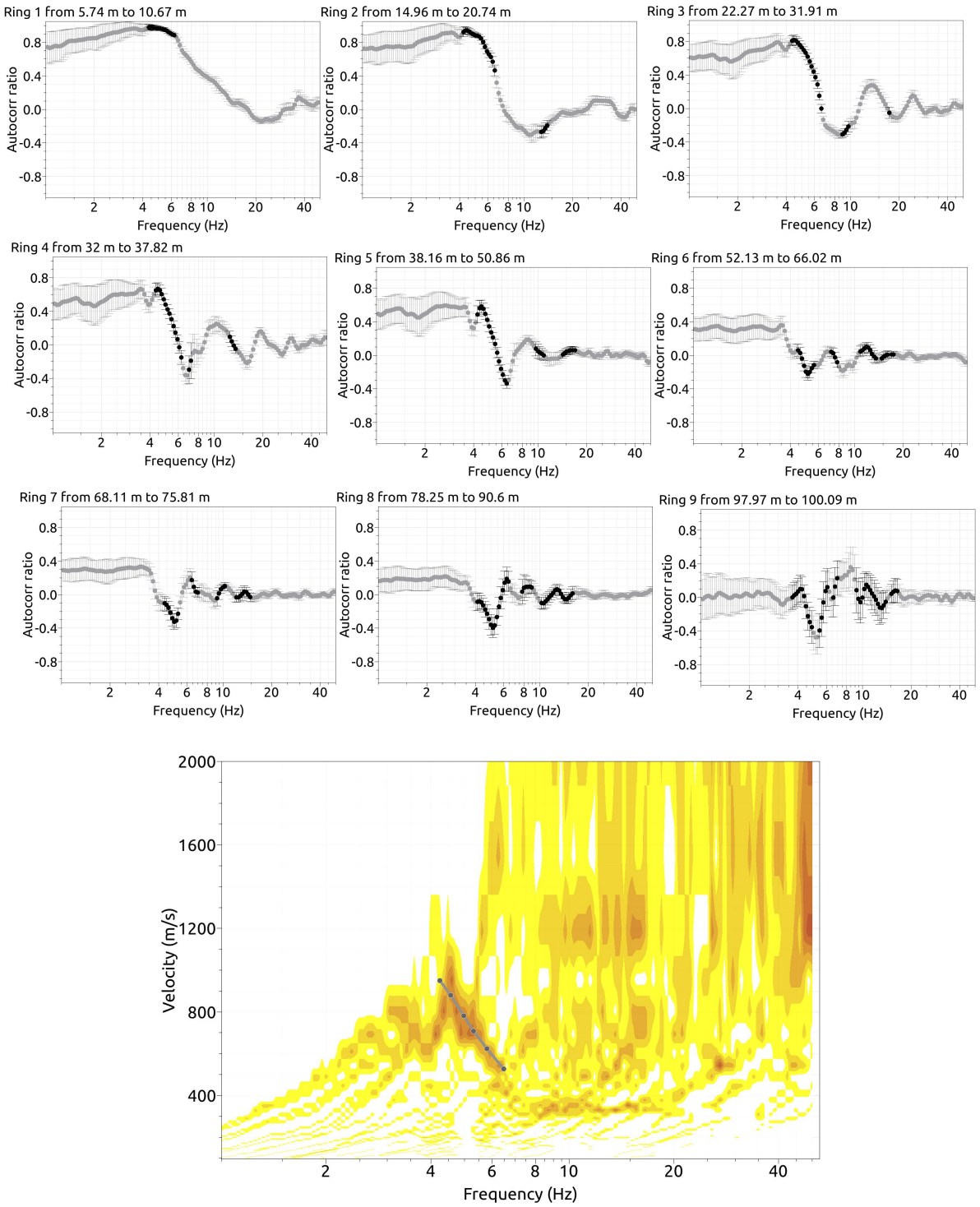

Figure 7: Top: M-SPAC results for the different rings. Bottom: Dispersion curve map with a clear dispersion curve branch between 4 and 7 Hz. The dispersion curve was estimated for a maximum co-array aperture of 100 m.

5.2 HRFK

Figure 8 shows the dispersion characteristic for Love waves on the transverse component and that of Rayleigh waves on the radial and vertical components. We picked one branch for the Love waves and two branches for Rayleigh on the radial and vertical components. The mode attribution was straightforward. We assume that the unique dispersion curve branch for Love waves is associated with the fundamental mode and the two dispersion curve branches for Rayleigh waves are associated with the fundamental and first higher mode, respectively.

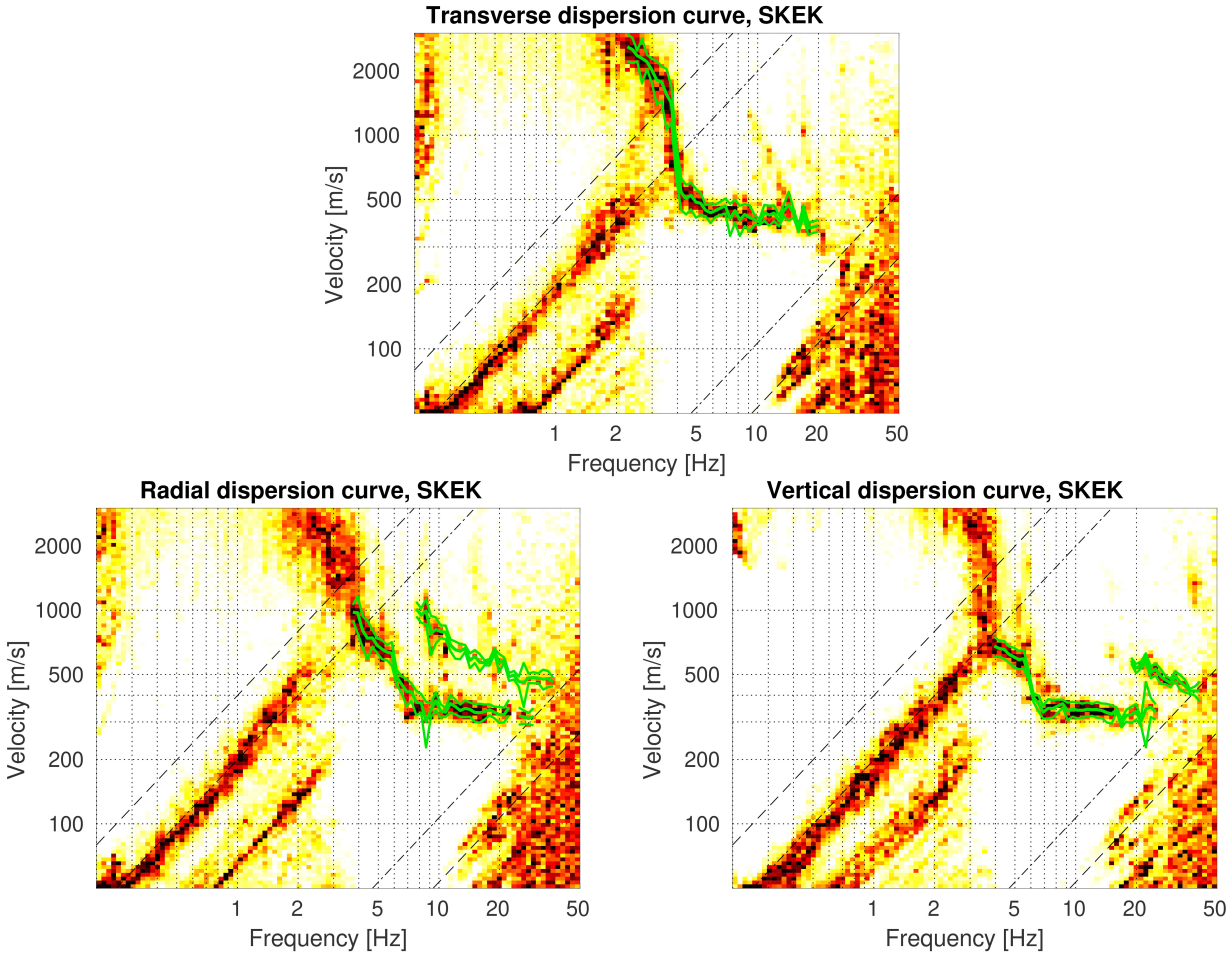

Figure 8: HRFK results. The phase velocity dispersion curves on the three components are shown. The phase velocity dispersion branches are picked on the transverse component for Love waves and on the vertical and radial components for Rayleigh waves. The dashed and dotted black lines are the array resolution limits. The solid green curves are picked from the data, where the central line indicates the best values and the two outer curves the standard deviation.

5.3 WaveDec

The WaveDec results are shown in Figure 9. We observe and pick one phase velocity dispersion branch for the Rayleigh and one branch for the Love waves. The ellipticity curve was picked in the frequency range of the Rayleigh wave dispersion curve and shows a prograde particle motion for frequencies below 6 Hz and a retrograde particle motion for frequencies above 6 Hz.

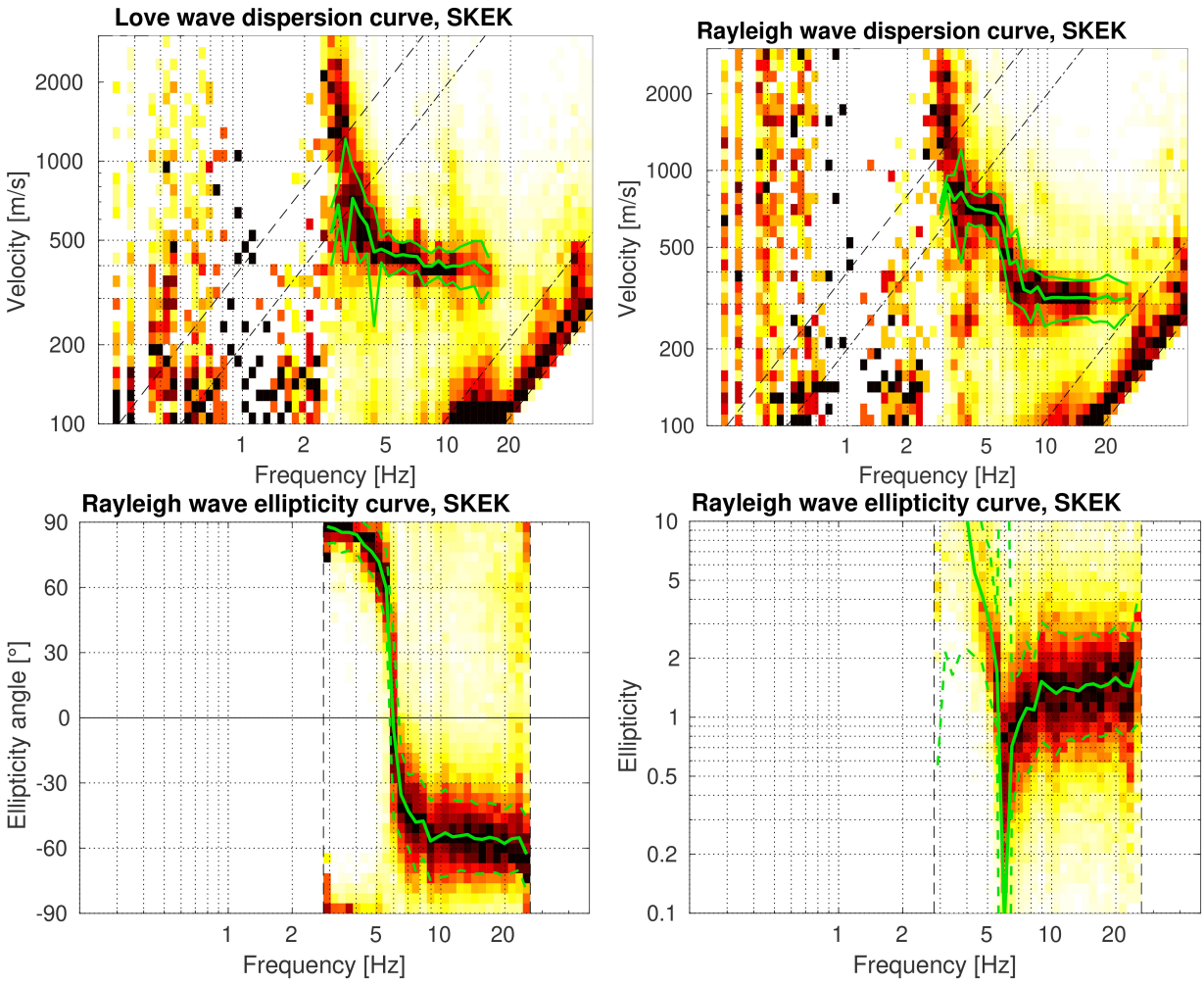

Figure 9: WaveDec results: ellipticity and phase velocity dispersion curves for Rayleigh and Love waves. The phase velocity dispersion branches are picked within the array resolution limits. The solid green curves are picked from the data, where the central line indicates the best values and the two outer curves the standard deviation.

5.4 Interferometric-Multichannel Analysis of Surface Waves (IMASW)

For the IMASW analysis, the correlation functions with 100 m maximum inter-station distance are used. For this maximum inter-station distance, a clear propagation of Rayleigh waves for the vertical component can be observed. Figure 10 shows the cross-correlation results and the resulting dispersion curve map. The dispersion characteristic of the Rayleigh waves is identified and manually picked.

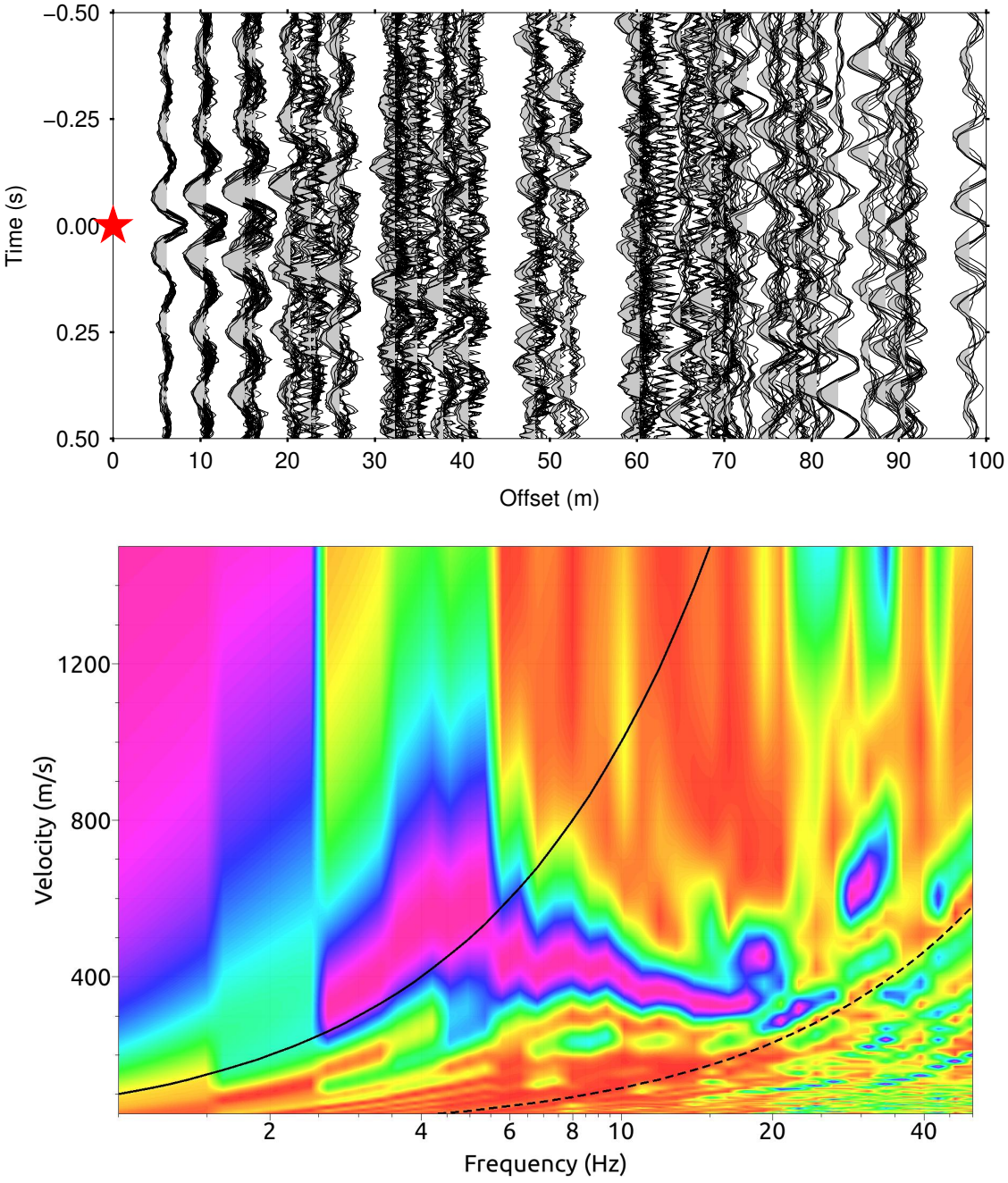

Figure 10: Top: Resulting cross-correlation Green's functions from receiver pair combinations with a maximum inter-station distance of 100 m (See array setup in Figure 2). The red star represents the virtual source. Bottom: frequency-wavenumber results from the cross-correlation functions. A clear phase velocity dispersion curve is observed in the frequency range between 6 and 20 Hz. The continuous and dashed lines define the resolution limits.

5.5 Overview and discussion of the measurement results

A summary of the estimated dispersion curve branches using the SPAC, HRFK, WaveDec, and IMASW methods is presented in Figure 11.
The Rayleigh wave branches for the fundamental mode obtained from SPAC and IMASW show slightly larger phase velocity values compared to the estimates from HRFK and WaveDec. The Rayleigh wave first higher mode is well developed on a large frequency range on the radial component compared to the vertical component. The dispersion curve from the radial component was then chosen and edited to remove picking artifacts and used as first higher mode in the inversion. The Love wave dispersion branches for the HRFK and WaveDec are in good agreement for frequencies above 5 Hz.
Based on preliminary inversion results, the fundamental mode was changed from HRFK to a combination of SPAC and IMASW dispersion curves. The first higher mode remained unchanged, but was edited to remove picking artifacts and corresponds to the dispersion curve on the HRFK radial component. The fundamental curve for Love waves was changed from WaveDec to HRFK that shows slightly larger phase velocity dispersion curve values.

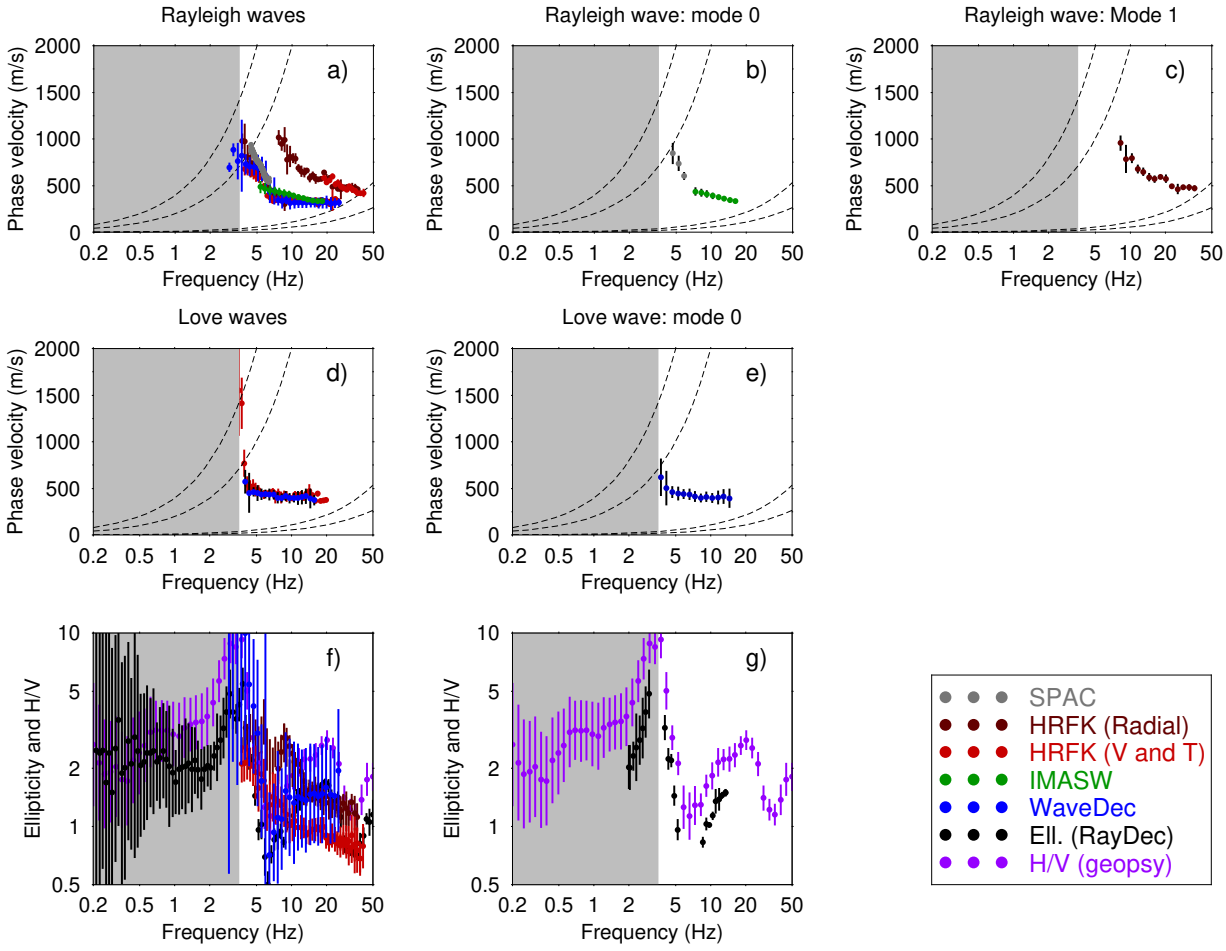

Figure 11: Overview of the results and interpreted curves obtained using the different analysis methods. a) Estimated Rayleigh wave dispersion curves. b) Interpreted Rayleigh wave phase velocity fundamental mode. c) Interpreted Rayleigh wave phase velocity first higher mode. d) Estimated Love wave dispersion curves. e) Interpreted Love wave phase velocity fundamental mode. f) Estimated microtremor H/V spectral ratio and Rayleigh wave ellipticity. g) Black dots indicate the fundamental mode ellipticity branches that were used in the inversion. Purple dots indicate the microtremor H/V spectral ratio used in the full-HV inversion. The gray box (see a-g) indicates additional frequency points from the ellipticity or H/V that are not covered by the dispersion curve. This additional information is useful in the inversion for constraining the bedrock depth and velocity.

6 Joint inversion of dispersion and ellipticity curves

6.1 Parametrization

The inversion assumes a layered earth structure. Three, four, five, six and seven layers over half-space were used, as well as a parameter space with fixed depths. The fixed-layer depth model consisted of 24 layers over half-space and the overall sediment cover was set to 300 m. The inversion uses the global search neighborhood algorithm (Sambridge, 1999; Wathelet, 2008). The process is started with a set of 50 models. In each iteration step, 50 new models are generated and the 50 best models are kept for further analysis. The process is iterated a large number of times, in this case 4000 times. This results in 200050 generated models. The choice of the parameters for the neighborhood algorithm ensures that we sufficiently explore and exploit the parameter space. The inversion process was repeated 10 times with different seeds and the inversion with the lowest minimum misfit was retained.

6.2 Inversion results

Figures 12-17 show the combined ellipticity and phase velocity dispersion curve inversion results. We summarize and interpret the best profiles from this inversion in Figure 18. Table 1 gives a summary of the minimum misfit values achieved in each inversion process.

Table 1: Minimum misfit values for different parametrizations.

Parametrization	Minimum misfit
3 LOH	0.580
4 LOH	0.557
5 LOH	0.556
6 LOH	0.546
7 LOH	0.552
Fixed layer depth	0.530

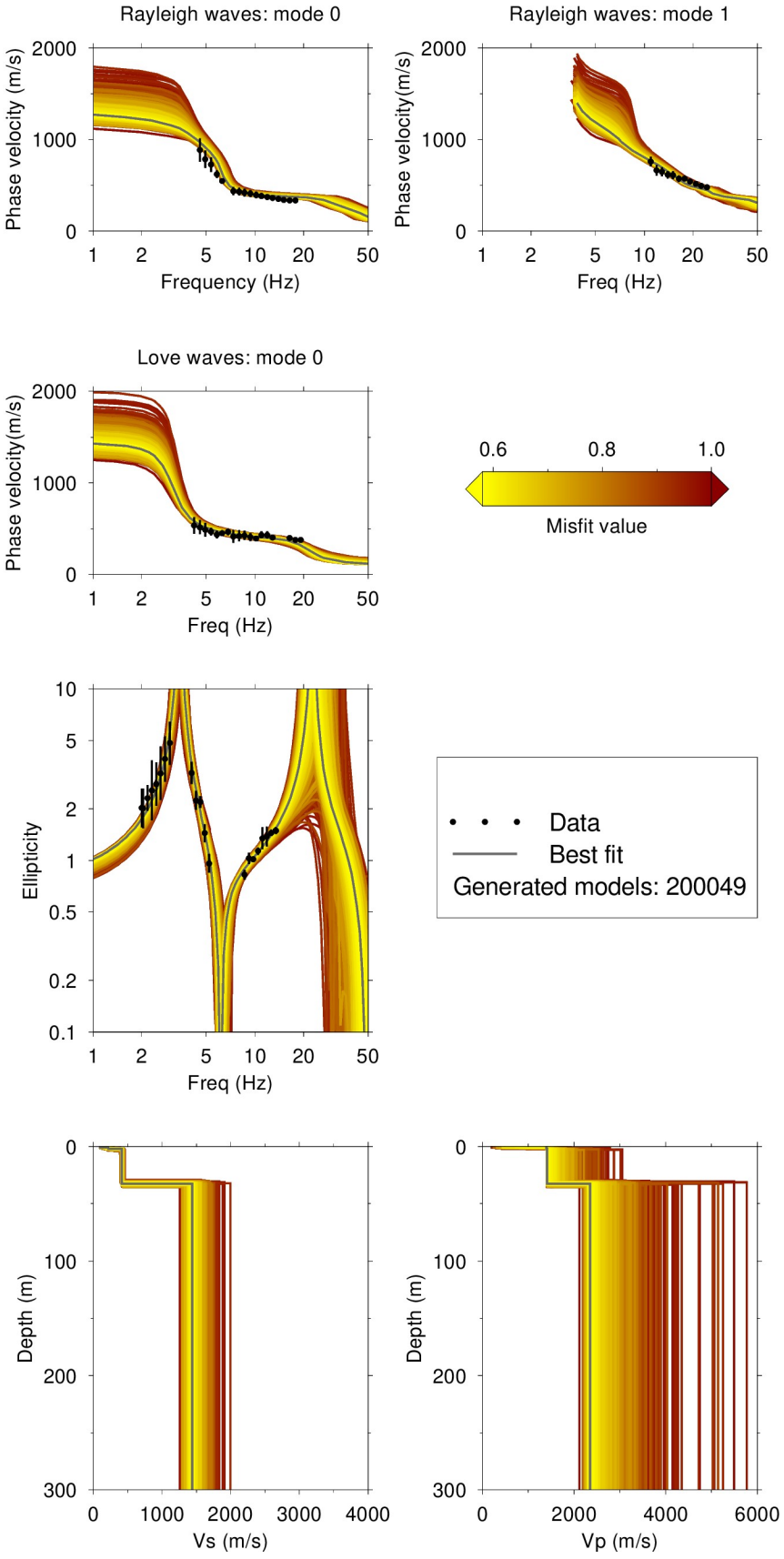

Figure 12: Inversion results using a 3LOH parametrization. The different models are shown in a color according to the misfit value, where the best model is shown in continuous gray color and the black dots indicate the data points that contribute to the inversion. The peak frequency is used as additional information to further constrain the bedrock depth and velocity.

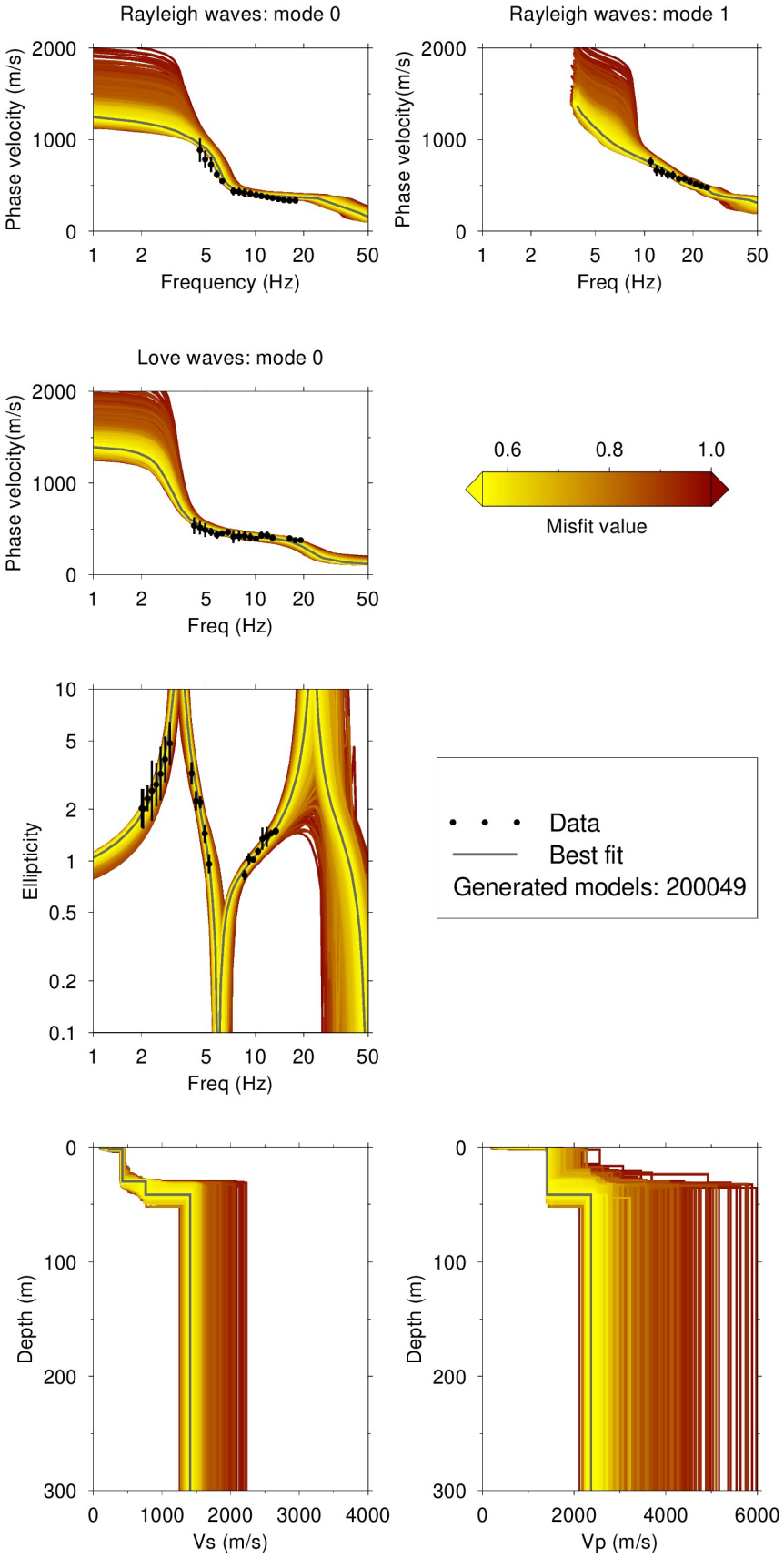

Figure 13: Inversion results using a 4LOH parametrization. The different models are shown in a color according to the misfit value, where the best model is shown in continuous gray color and the black dots indicate the data points that contribute to the inversion. The peak frequency is used as additional information to further constrain the bedrock depth and velocity.

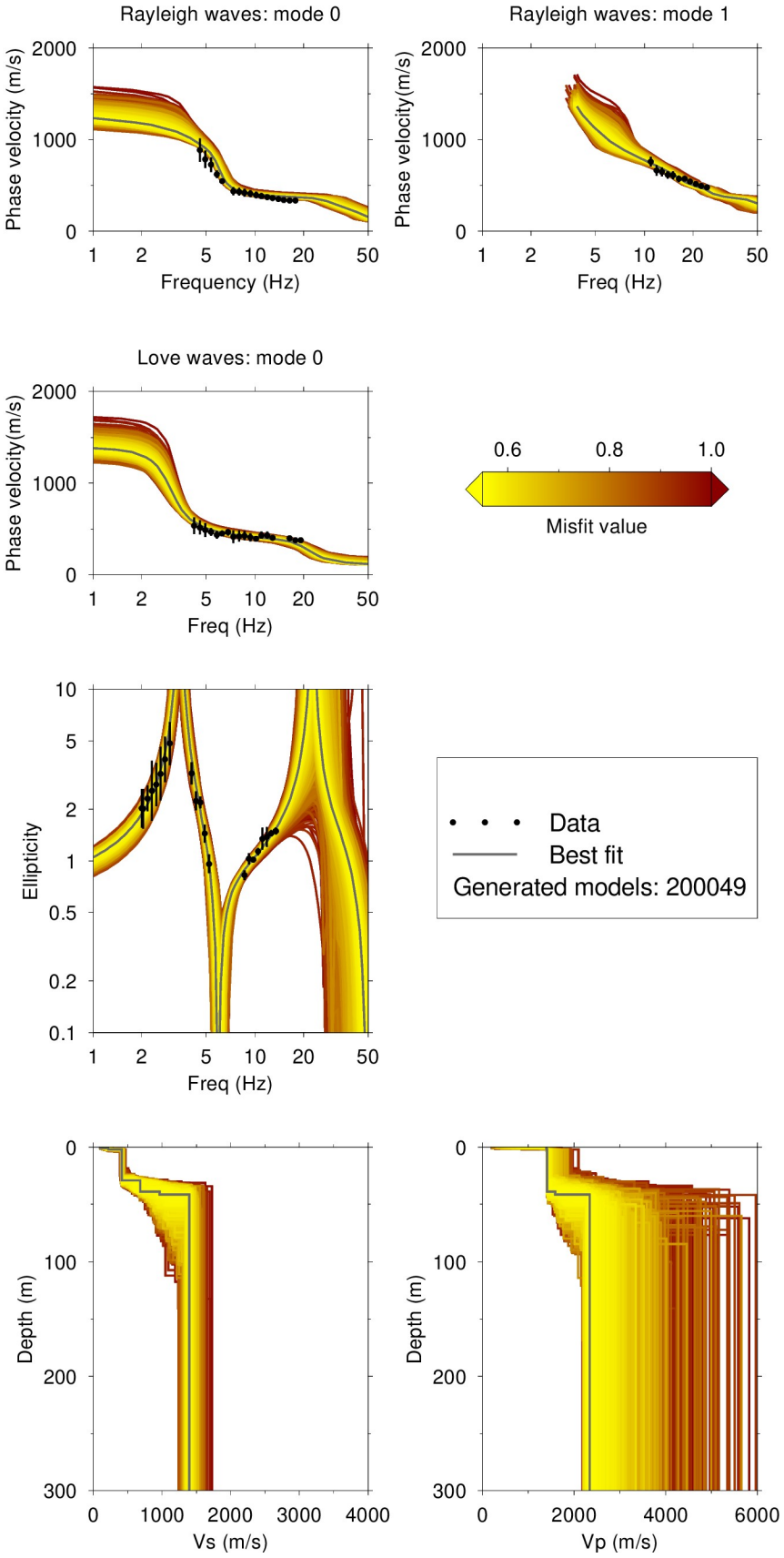

Figure 14: Inversion results using a 5LOH parametrization. The different models are shown in a color according to the misfit value, where the best model is shown in continuous gray color and the black dots indicate the data points that contribute to the inversion. The peak frequency is used as additional information to further constrain the bedrock depth and velocity.

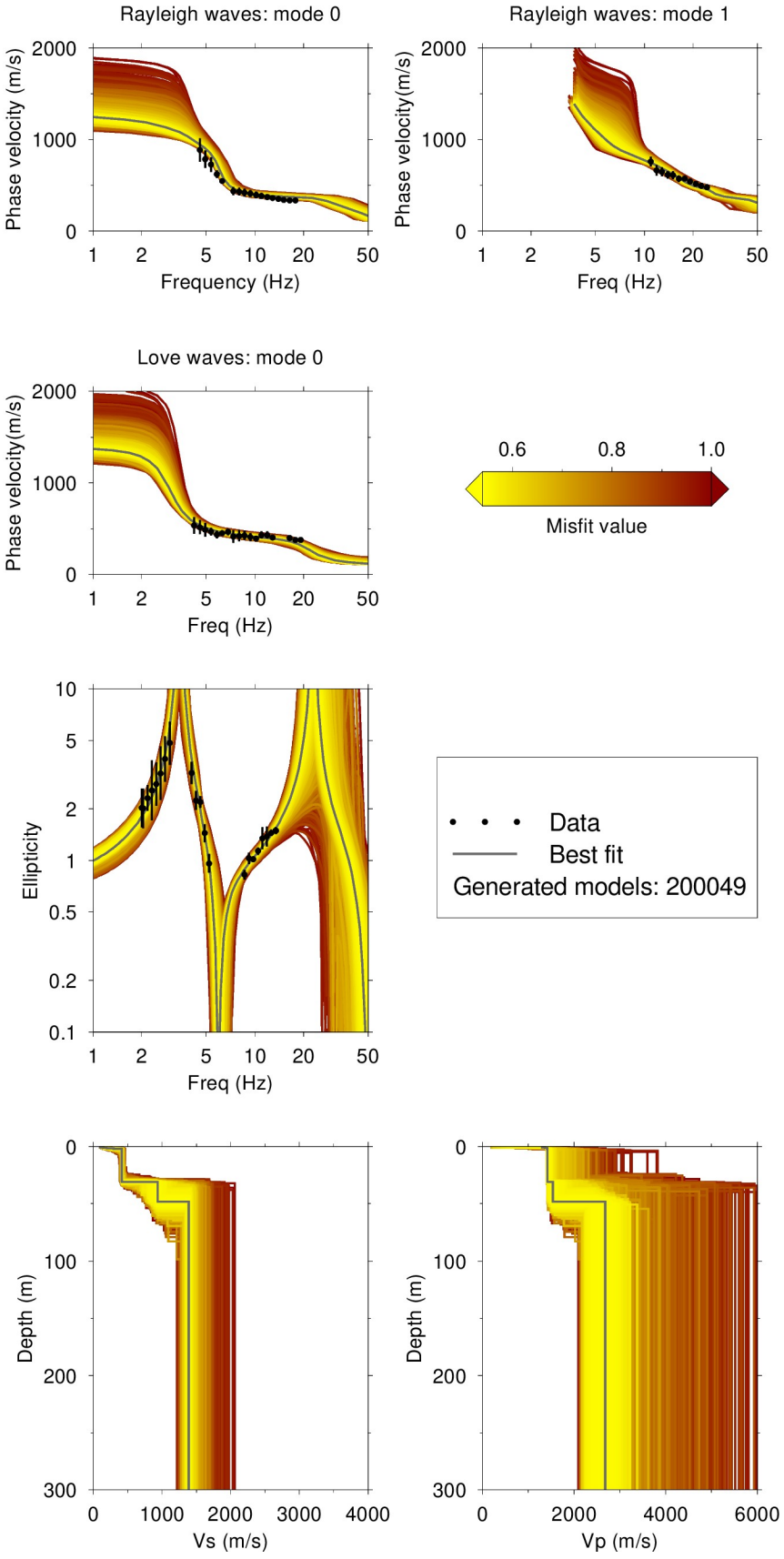

Figure 15: Inversion results using a 6LOH parametrization. The different models are shown in a color according to the misfit value, where the best model is shown in continuous gray color and the black dots indicate the data points that contribute to the inversion. The peak frequency is used as additional information to further constrain the bedrock depth and velocity.

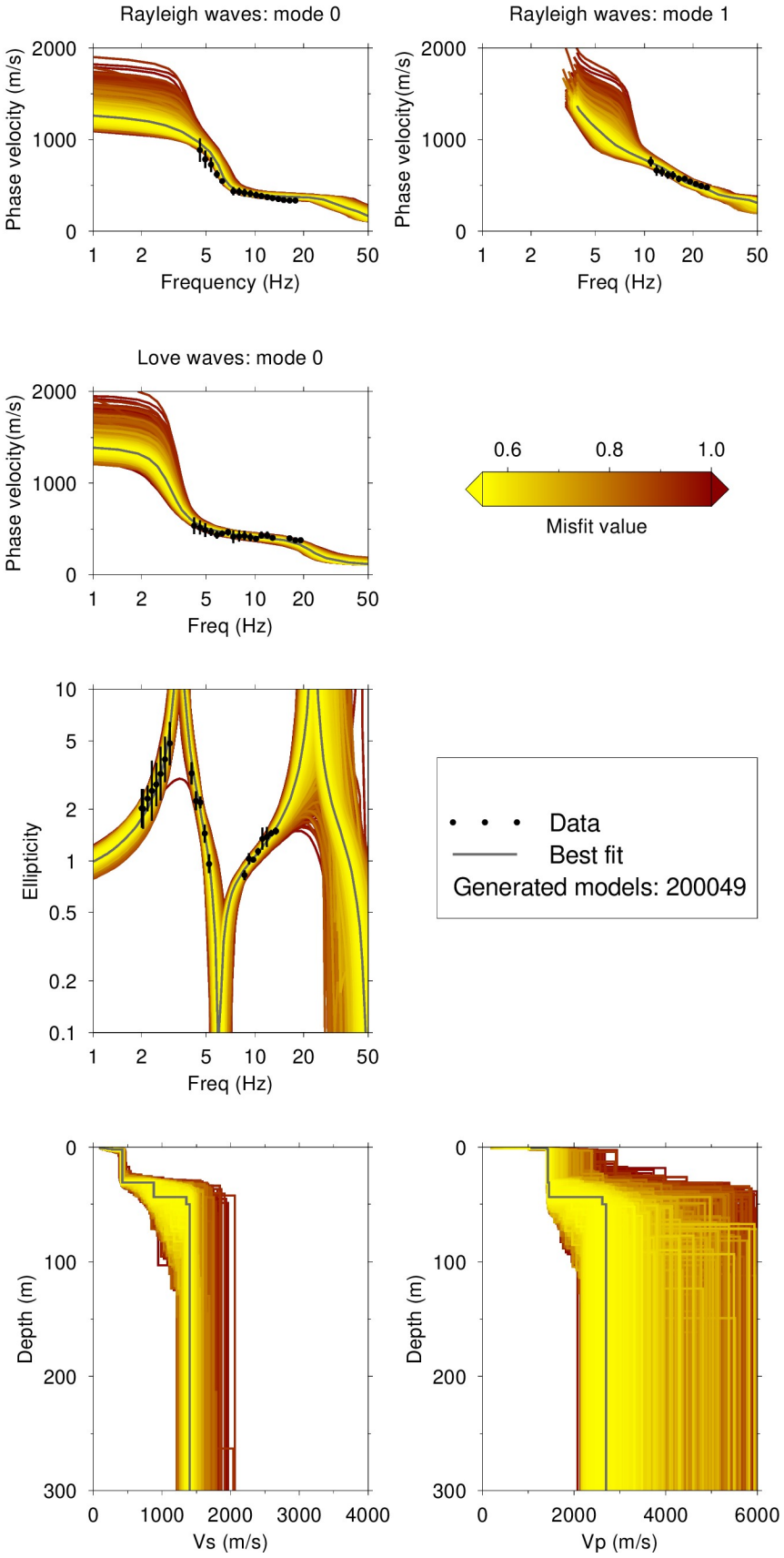

Figure 16: Inversion results using a 7LOH parametrization. The different models are shown in a color according to the misfit value, where the best model is shown in continuous gray color and the black dots indicate the data points that contribute to the inversion. The peak frequency is used as additional information to further constrain the bedrock depth and velocity.

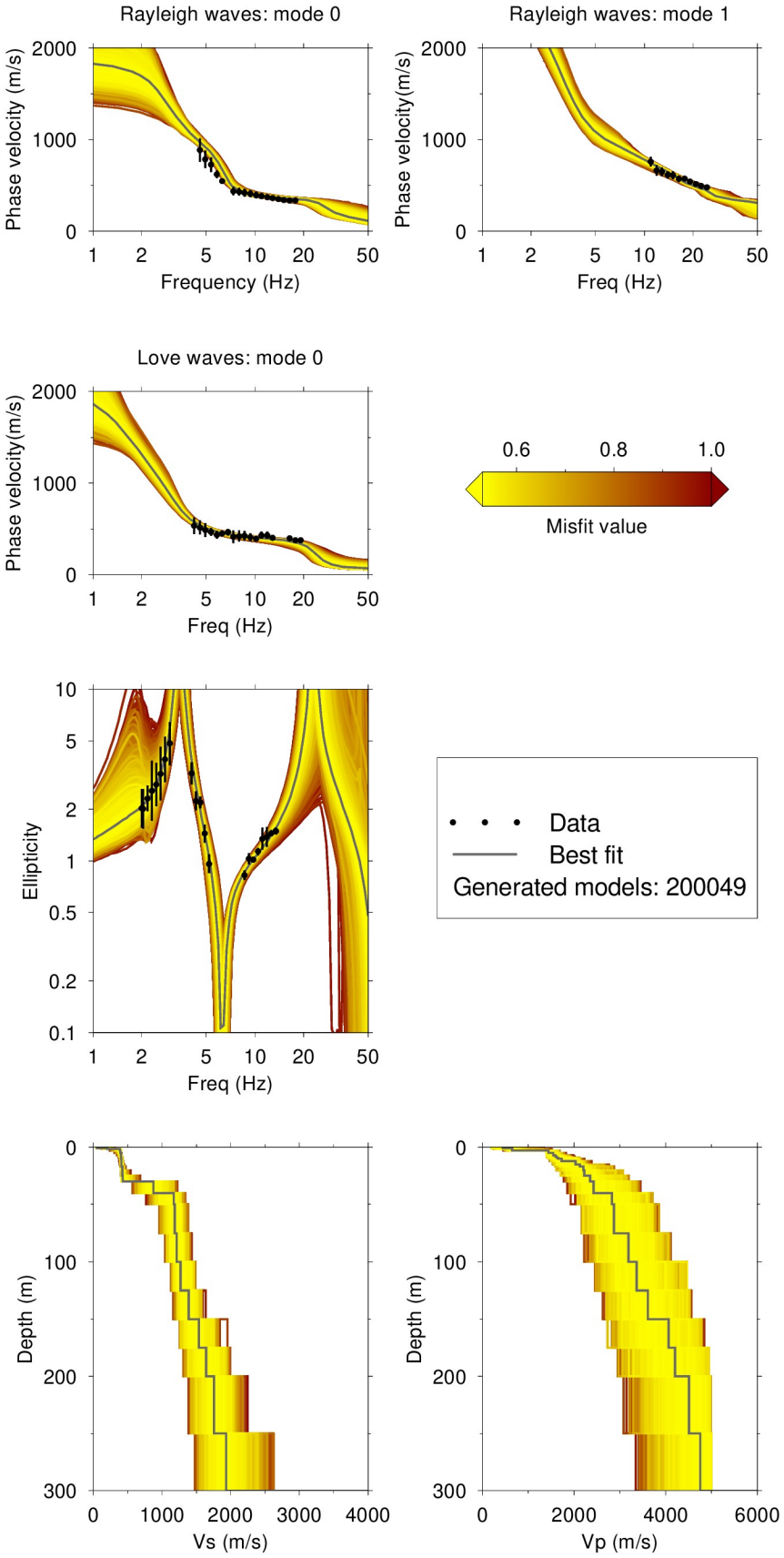

Figure 17: Inversion results using a FixedLayer thickness parametrization. The different models are shown in a color according to the misfit value, where the best model is shown in continuous gray color and the black dots indicate the data points that contribute to the inversion. The peak frequency is used as additional information to further constrain the bedrock depth and velocity.

6.3 Inversion summary

The best models from the inversions using different parametrizations (3LOH, 4LOH, 5LOH, 6LOH, 7LOH, and FixedLayer) are shown in Figure 18.
The misfit values from the combined inversion vary between 0.53 and 0.58. A comparison of the velocity profiles indicates that there is a velocity gradient between 30 and 50 m depth. The average V_{S30} from the six best models in the surface wave inversion is 371 $\pm$ 4 m/s. This V_{S30} value corresponds to ground type B in EC8 (European standard) and to ground type C in SIA261 (Swiss standard).

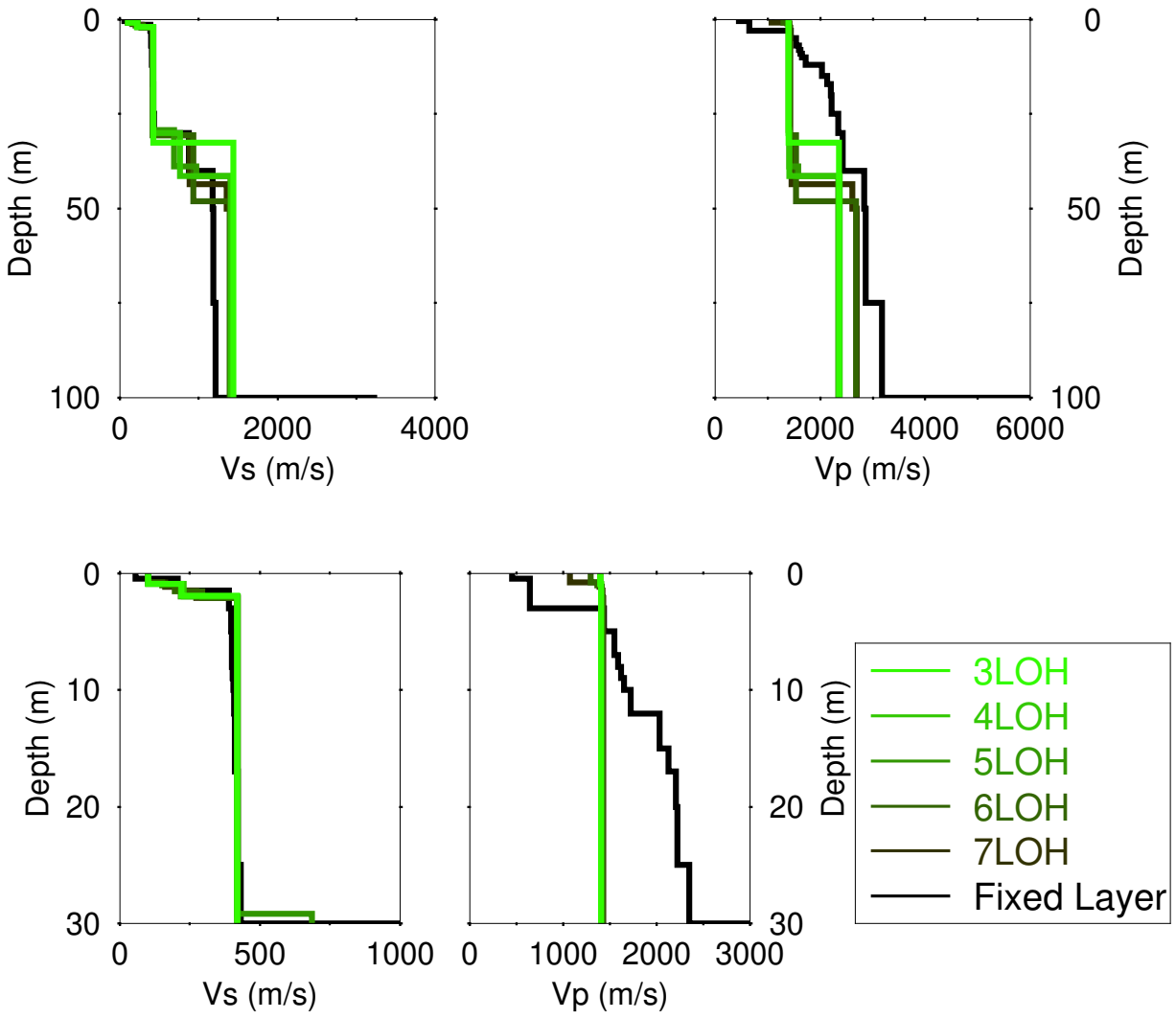

Figure 18: Overview of the best models for the different parameterizations. Top: S-wave (left) and P-wave (right) velocity profiles. Bottom: Zoom on the superficial 30 meters.

6.4 Site amplification

Starting from the best models presented in Figure 18, the theoretical site amplification function is computed and compared with the empirical site amplification function of the station SKEK. The amplification is further calibrated by the one for the Swiss reference profile. The site amplification function is estimated following Edwards et al. (2013). The comparison is shown in Figure 19. In addition, the full-HV algorithm (Lontsi et al., 2019) is used to model the H/V curve.
The overall shapes of the H/V, empirical and theoretical amplification functions retrieve the peak frequencies up to about 15 Hz. Within the uncertainties, the absolute amplification at the major peak frequency at 3.63 Hz is well retrieved by all approaches.

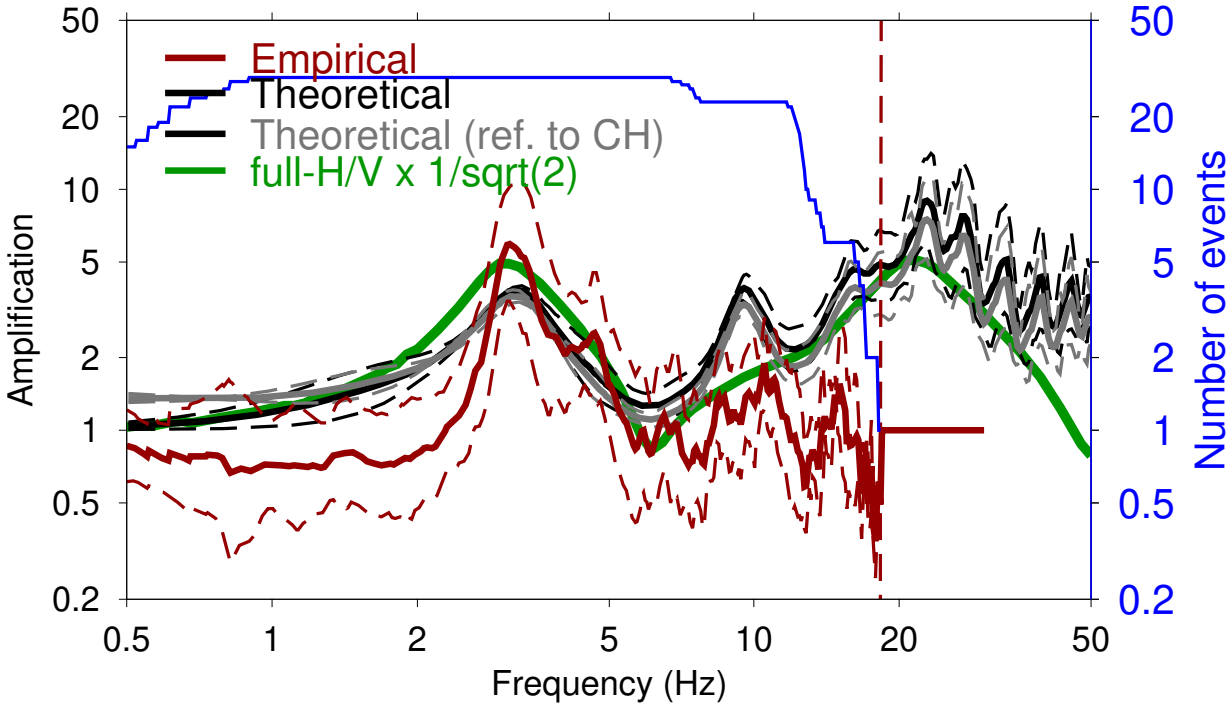

Figure 19: Comparison between the site amplification estimated for the best models from the inversions and the empirical amplification for station SKEK. In addition, the amplification function referenced to the Swiss reference profile and the full H/V spectral ratio curves are plotted.

6.5 Quarter-wavelength representation

The quarter wavelength representation for the joint inversion of ellipticity and dispersion curves is presented in Figure 20. The depth resolution is estimated to approximately 100 m.

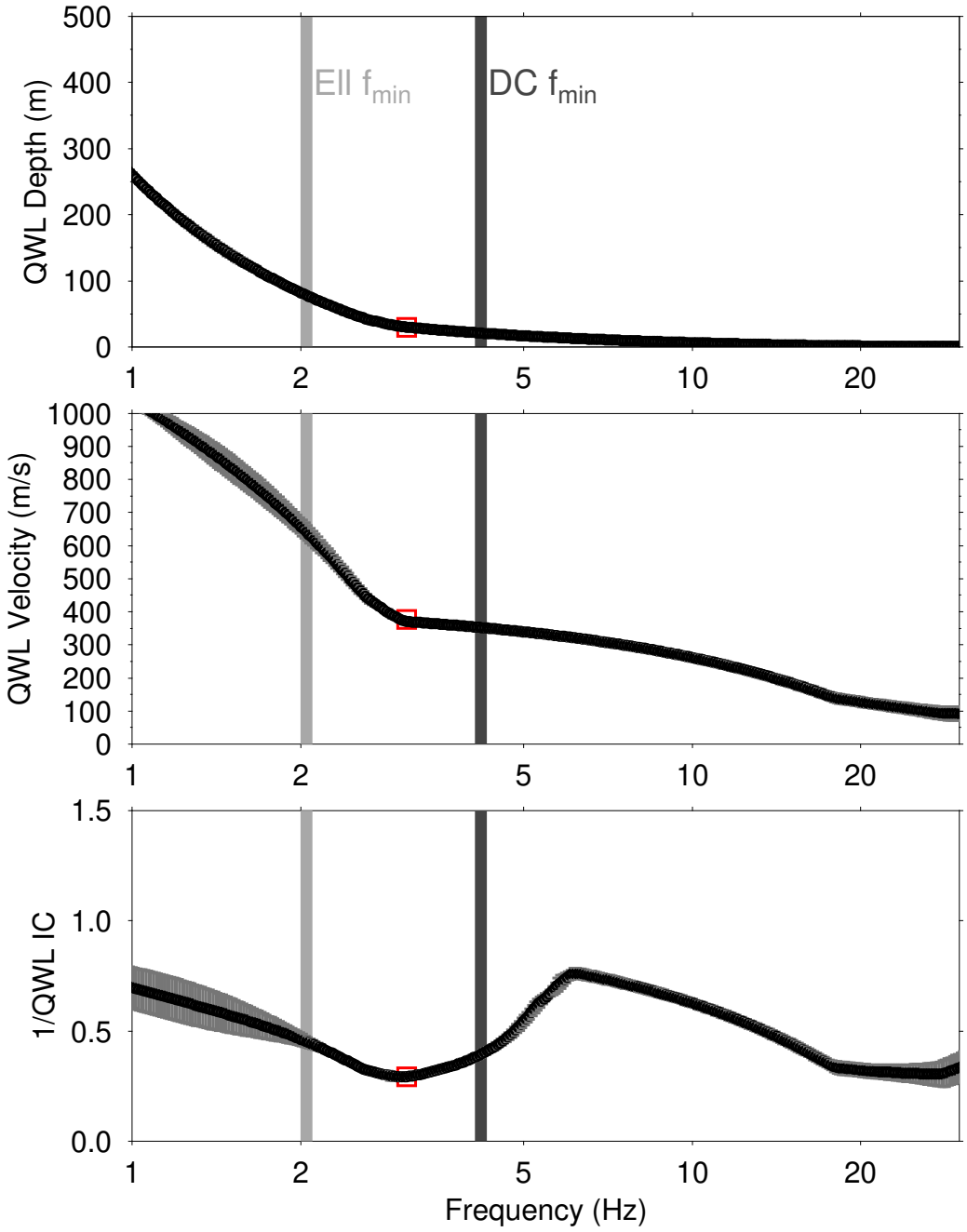

Figure 20: Quarter-wavelength representation for the best models of the inversions. The light and dark gray vertical bars indicate the minimum frequencies for the ellipticity and phase velocities, respectively, used in the inversion process. The solid black line uses all models of Figure 18.

7 Joint inversion of full H/V and phase velocity dispersion curves

7.1 Parametrization

Similar to the joint inversion of dispersion and ellipticity curves, the inversion assumes a layered earth structure. Three, four, five, six and seven layers over half-space were used. No parameter space with fixed depths was tested.

7.2 Results

Figures 21-25 show the full-HV inversion results. We summarize and interpret the best profiles from the inversion in Figure 26. Table 2 gives a summary of the minimum misfit values achieved in each case during the inversion process.

Table 2: Minimum misfit values for different parametrizations.

Parametrization	Minimum misfit
3 LOH	0.511
4 LOH	0.483
5 LOH	0.481
6 LOH	0.488
7 LOH	0.502

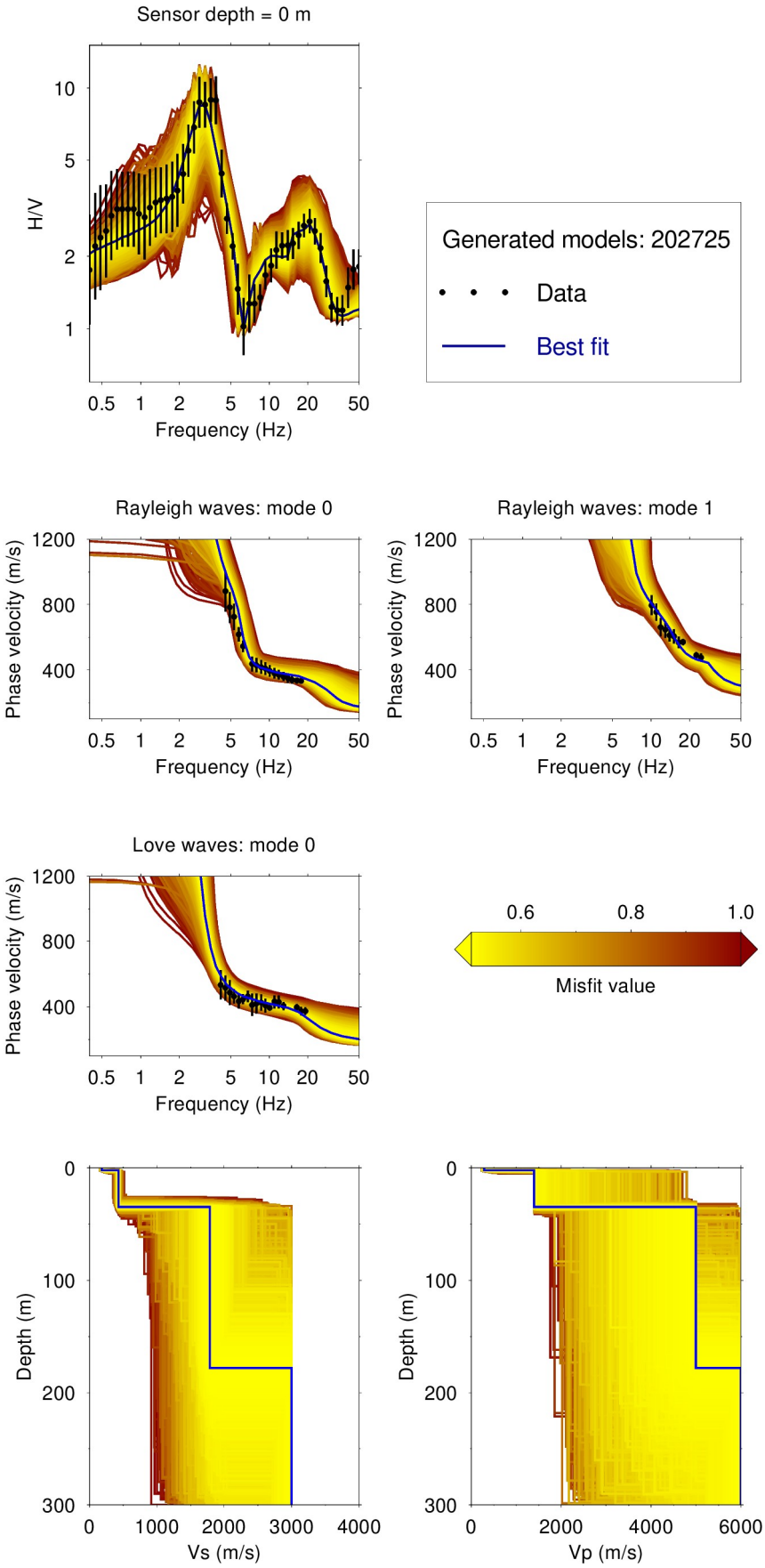

Figure 21: Full-HV inversion results using a 3LOH parametrization. The different models are shown in a color according to the misfit value, where the best model is shown in continuous blue color and the black dots indicate the data points that contribute to the inversion.

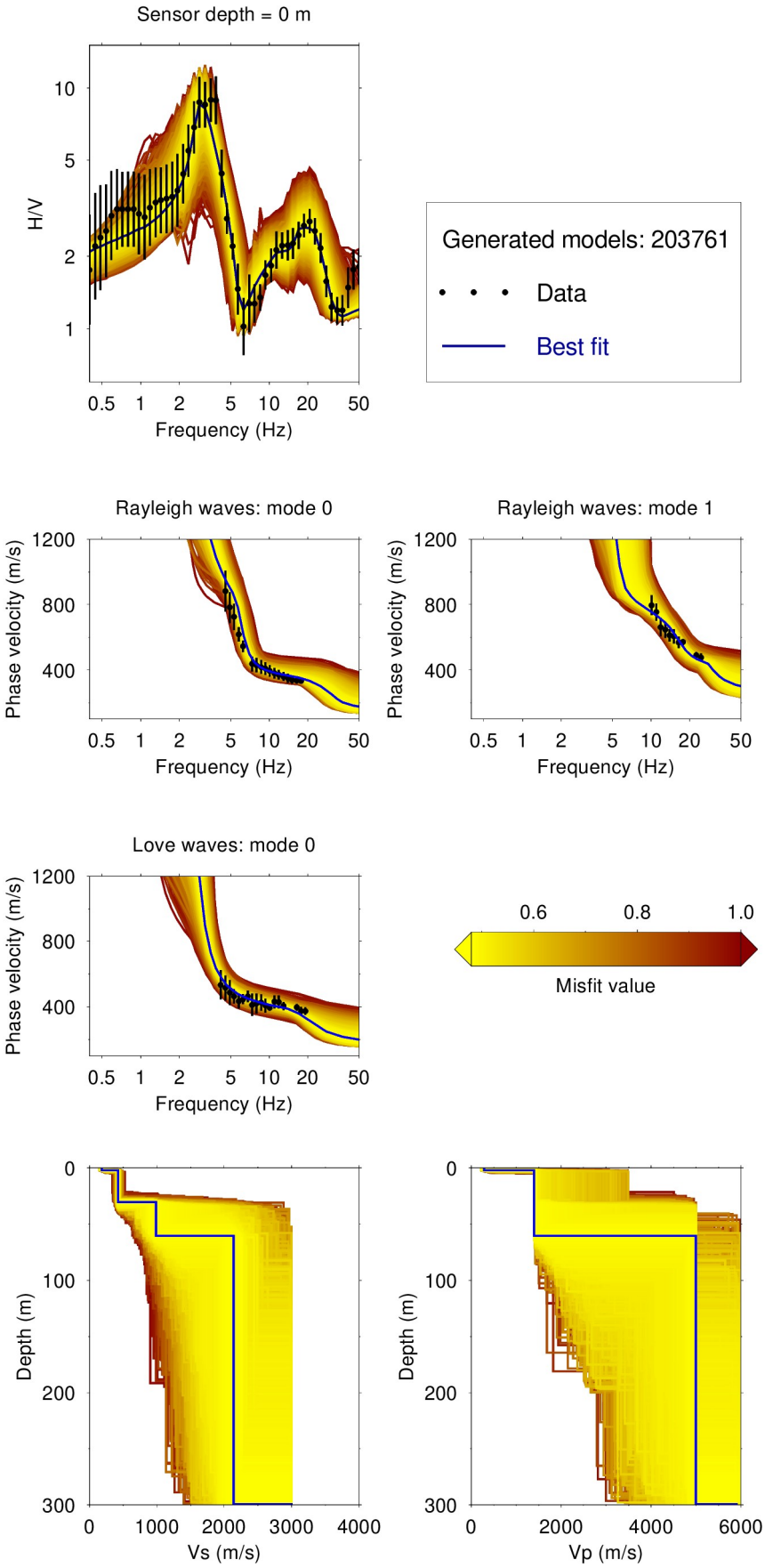

Figure 22: Full-HV inversion results using a 4LOH parametrization. The different models are shown in a color according to the misfit value, where the best model is shown in continuous blue line and the black dots indicate the data points that contribute to the inversion.

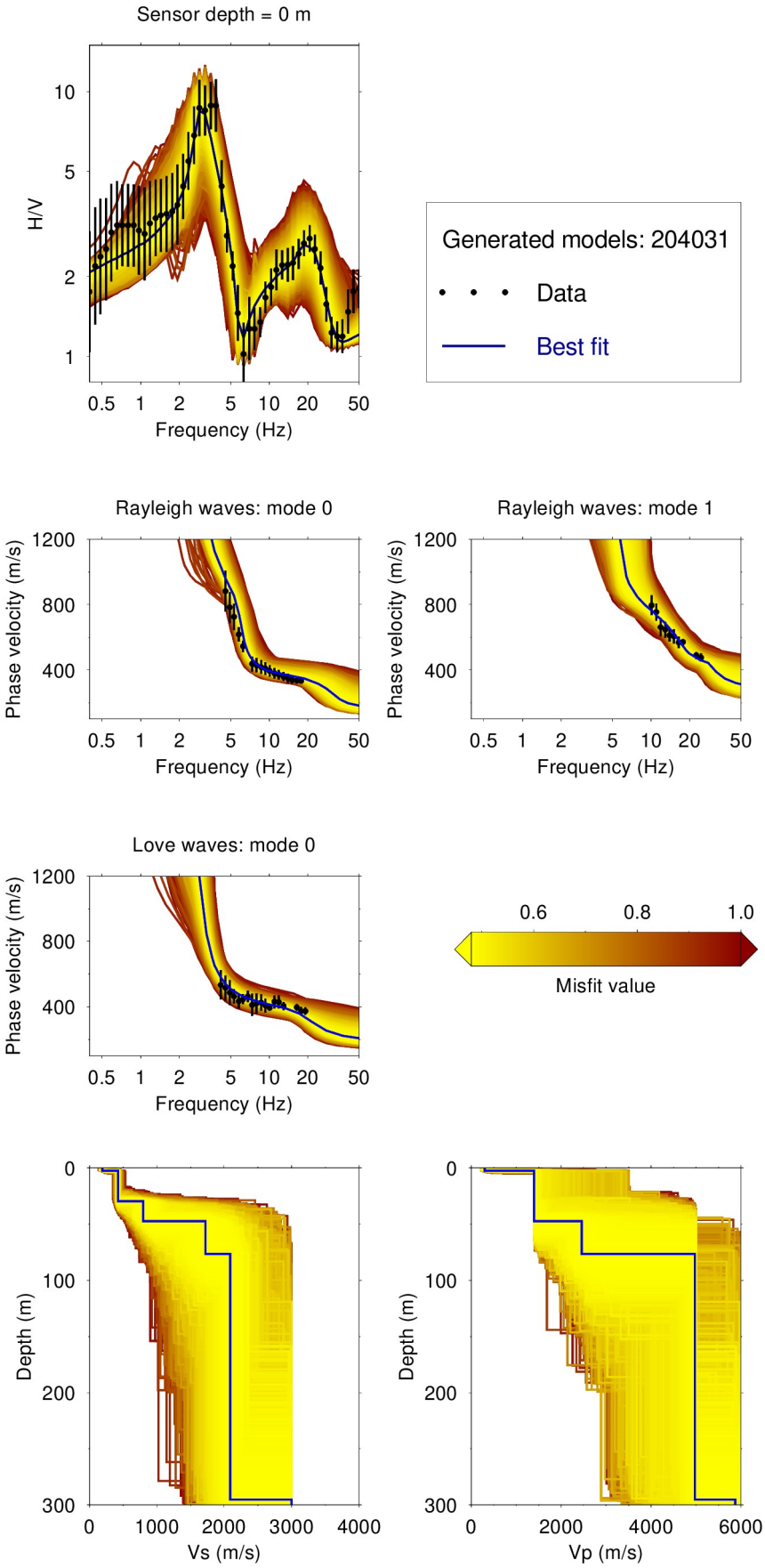

Figure 23: Full-HV inversion results using a 5LOH parametrization. The different models are shown in a color according to the misfit value, where the best model is shown in continuous blue line and the black dots indicate the data points that contribute to the inversion.

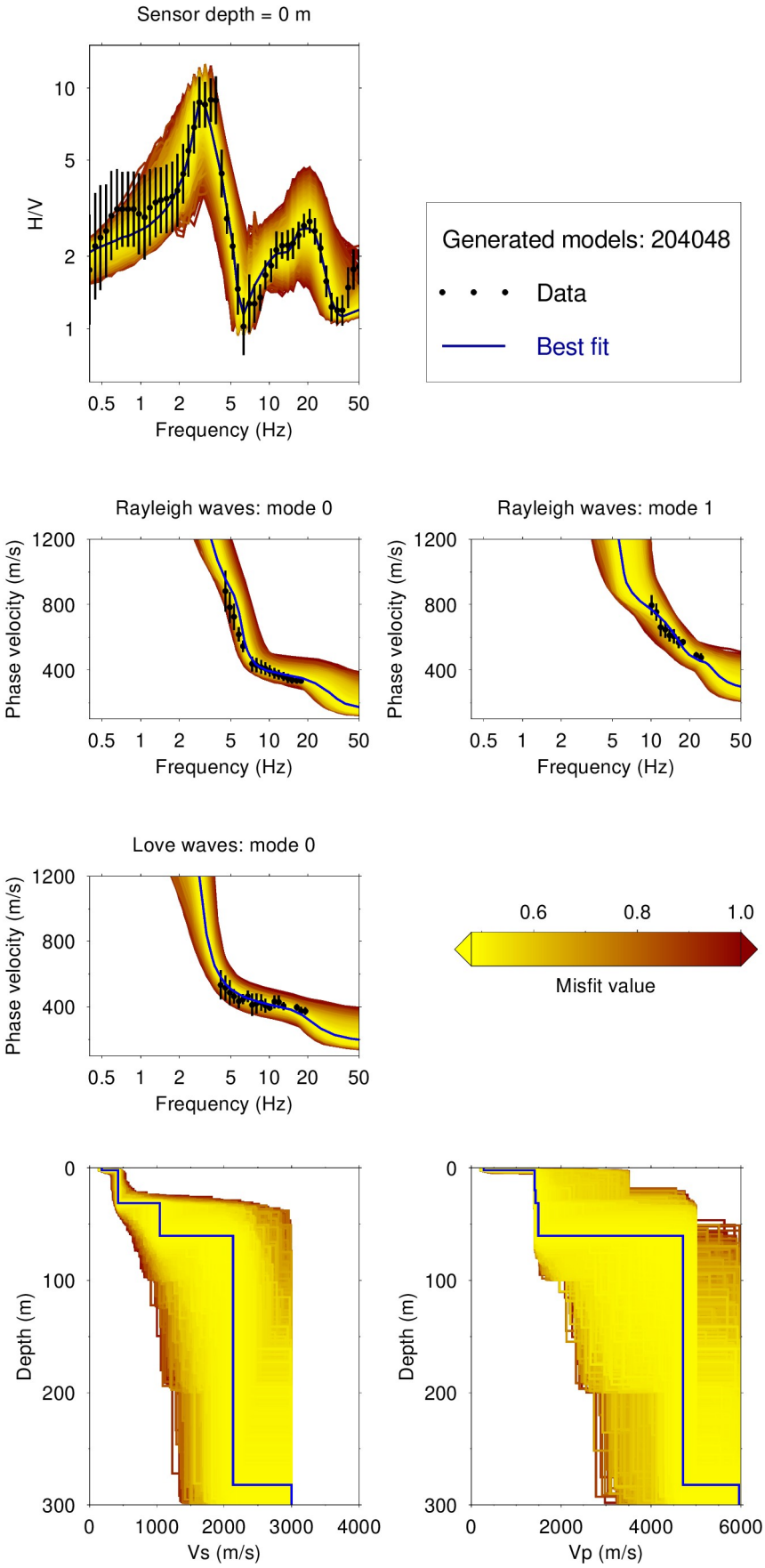

Figure 24: Full-HV inversion results using a 6LOH parametrization. The different models are shown in a color according to the misfit value, where the best model is shown in continuous blue line and the black dots indicate the data points that contribute to the inversion.

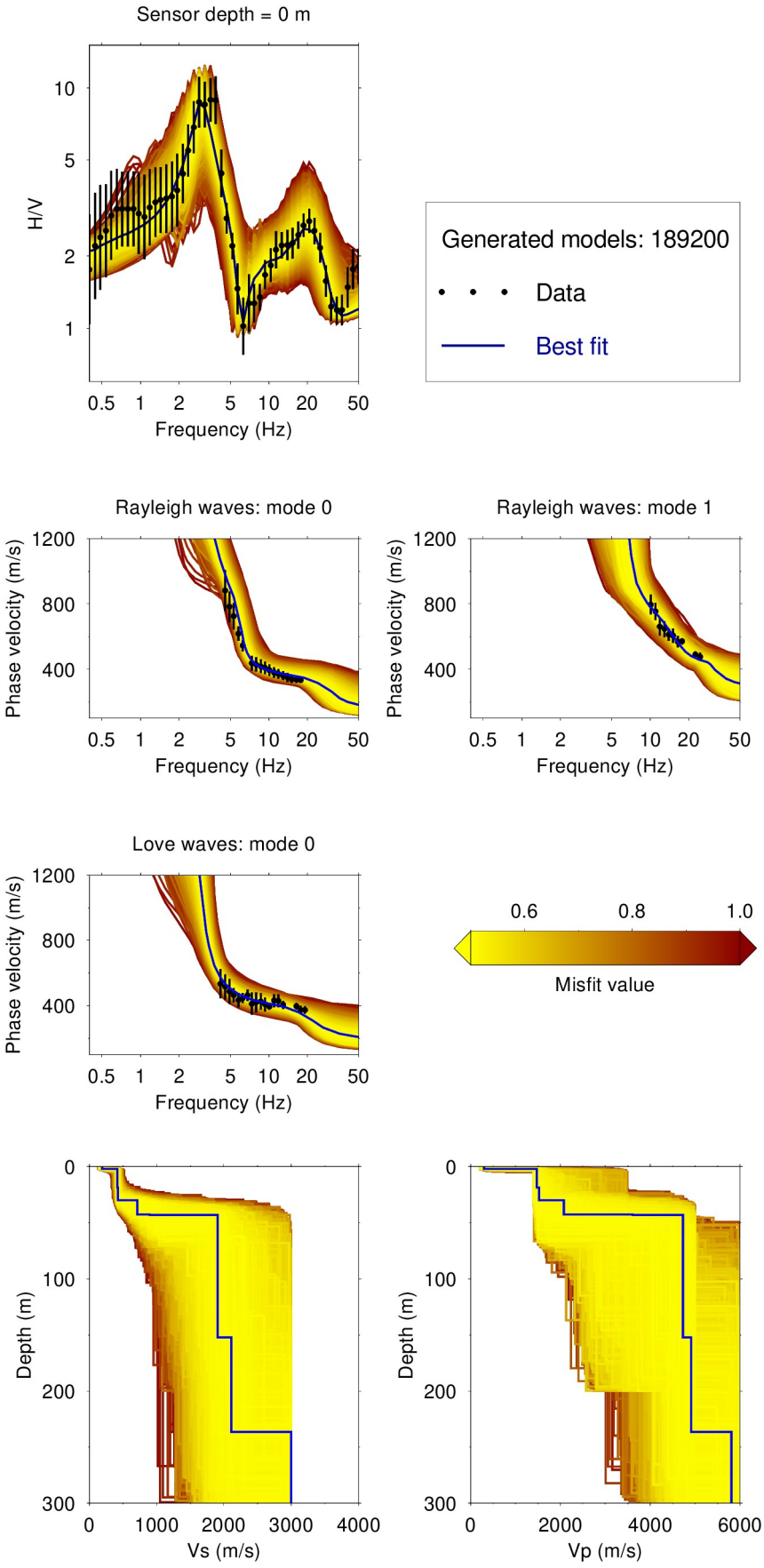

Figure 25: Inversion results using a 7LOH parametrization. The different models are shown in a color according to the misfit value, where the best model is shown in continuous blue line and the black dots indicate the data points that contribute to the inversion.

7.3 Inversion summary

The best models from the inversions using different parametrizations (3LOH, 4LOH, 5LOH, 6LOH, and 7LOH) are shown in Figure 26.

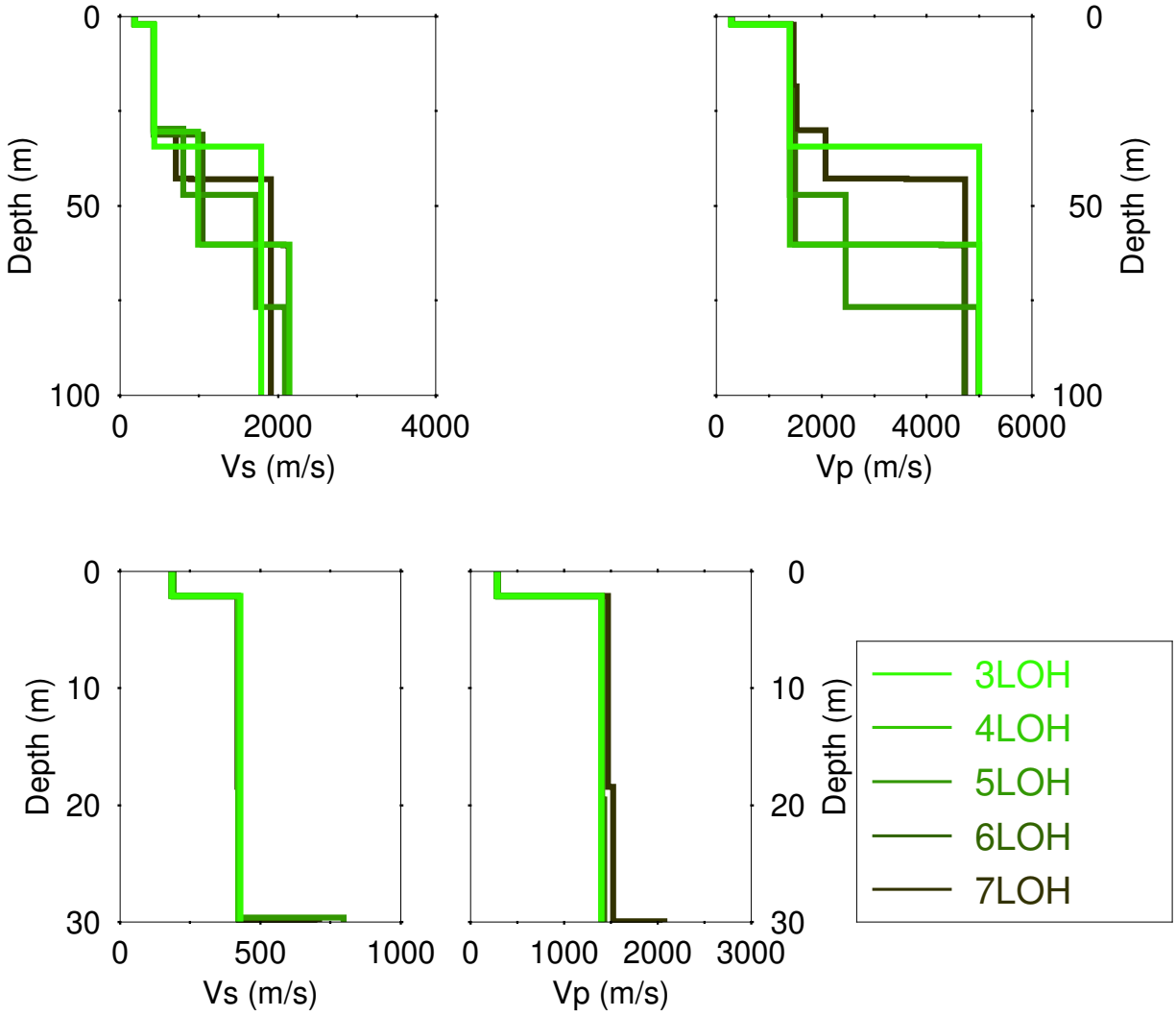

Figure 26: Overview of the best models for the different parameterizations. Top: S-wave (left) and P-wave (right) velocity profiles. Bottom: Zoom on the superficial 30 meters.

The misfit values from the combined inversion vary between 0.481 and 0.511. The average V_{S30} value is 388 $\pm$ 3 m/s. This V_{S30} value is comparable to the previous one and corresponds to ground type B in EC8 (European standard) and to ground type C in SIA261 (Swiss standard).

7.4 Site amplification

Starting from the models presented in Figure 26, the theoretical site amplification function is computed and compared with the empirical site amplification function of the station SKEK. The site amplification function is estimated following Edwards et al. (2013). The comparison is shown in Figure 27.
The curves very good agreement between the full-HV curves and the empirical amplification function. The SH transfer function overestimates the amplification in the high frequency above 5 Hz.

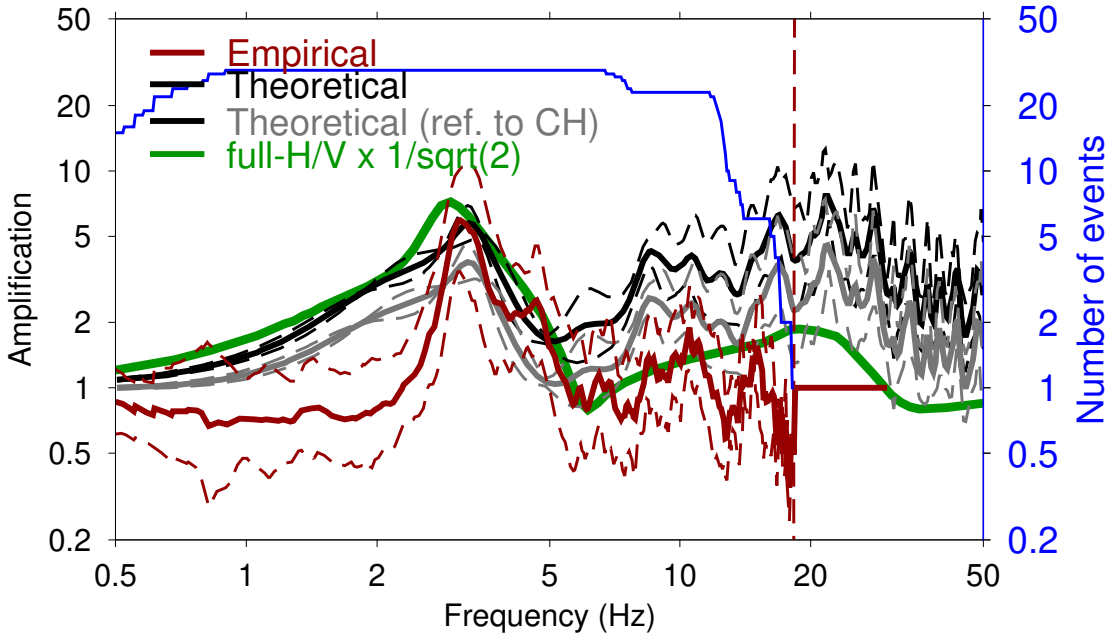

Figure 27: Comparison between the site amplification estimated for the best models from the inversions and the empirical amplification for station SKEK.

7.5 Quarter-wavelength representation 2

The quarter wavelength representation for the joint inversion of full-HV and dispersion curves is presented in Figure 28. The depth resolution is estimated to approximately 1500 m. This is a large value compared for the analyzed frequency range for H/V curves. A look at the H/V inversion results allows to see a very good fit down to about 1 Hz which corresponds to a depth resolution down to about 300 m.

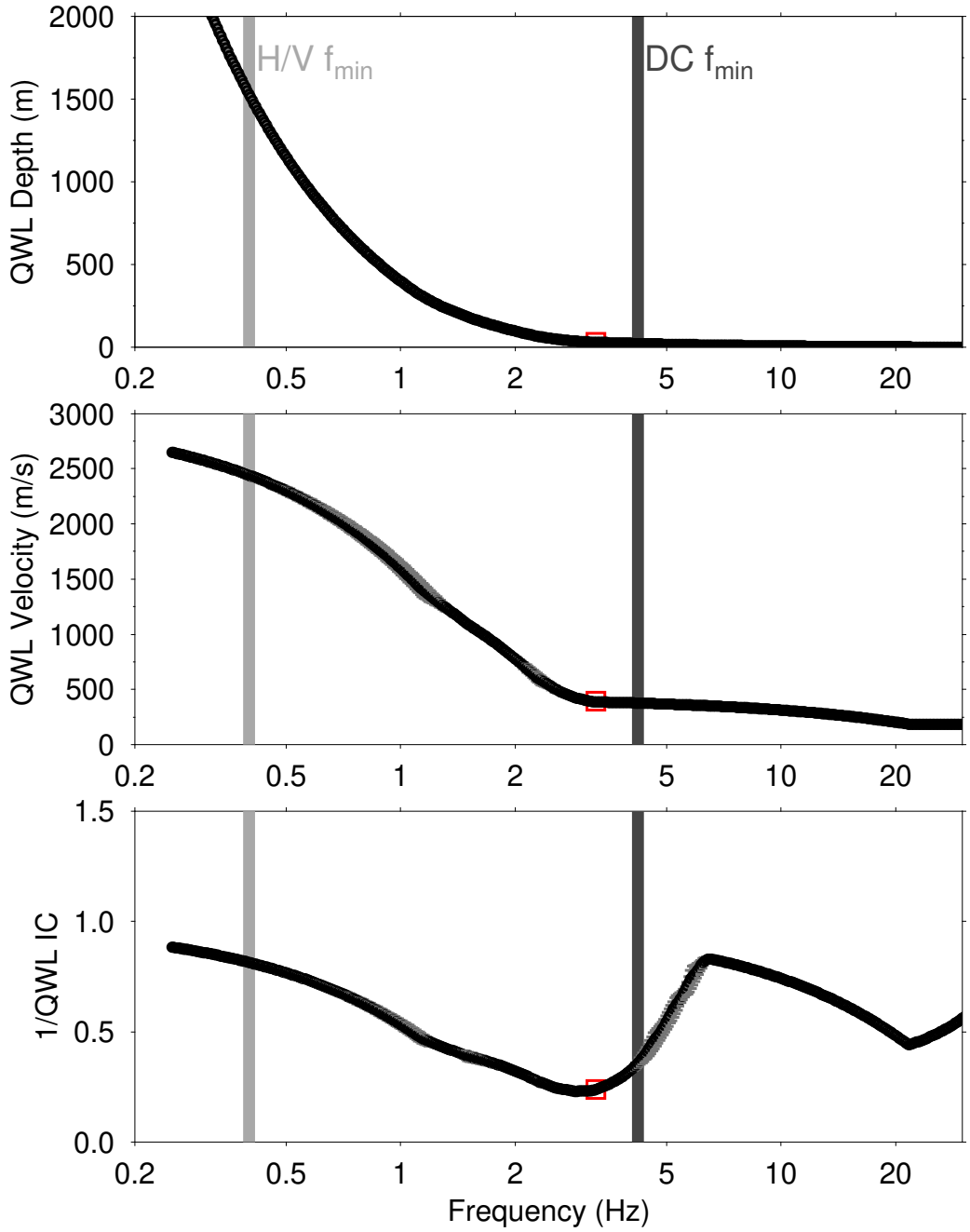

Figure 28: Quarter-wavelength representation for the best models of the inversions. The light and dark gray vertical bars indicate the minimum frequencies for the ellipticity and phase velocities, respectively, used in the inversion process. The solid black line uses the models of Figure 26.

8 Conclusion

A passive seismic survey was carried out at the strong motion station SKEK at Kerns (OW) to characterize the local subsurface. The dispersion curves for Love and Rayleigh waves were estimated over a wide frequency band ranging from 4.2 Hz to 24.4 Hz. Two frequency peaks were measured for the H/V spectral ratio and ellipticity at around 0.7 and 3.6 Hz, where the peak at 3.6 Hz is the dominant peak. The array methods used were complementary in selecting the appropriate dispersion curve branch for the fundamental mode Rayleigh waves. Both inversions were able to estimate the bedrock depth between 30 and 75 m and the V_{S30} values 371 ± 4 m/s and 388 ± 3 m/s. The ground is classified as ground type B in EC8 (European standard) and ground type C in SIA261 (Swiss standard). Below 75 m depth, full-HV inversion gives a large bedrock shear wave velocity of about 2000 m/s compared to 1400 m/s from the ellipticity inversion. It is also observed that the amplitude of the full-HV curve from the best model of inversion 2 shows a good comparison with the empirical amplification in terms of amplitude on a broad frequency range compared to the theoretical SH-transfer function.

9 Acknowledgments

Manuel Studer helped during the array measurements.

References

Aki, K., 1957. Space and time spectra of stationary stochastic waves, with special reference to microtremors., *Bull. Earthq. Res. Inst.*, **35**, 415–456.

Bettig, B., Bard, P. Y., Scherbaum, F., Riepl, J., Cotton, F., Cornou, C., & Hatzfeld, D., 2001. Analysis of dense array noise measurements using the modified spatial auto-correlation, *Boll. Geof. Teor. Appl.*, **42**, 281–304.

Burjánek, J., Gassner-Stamm, G., Poggi, V., Moore, J. R., & Fäh, D., 2010. Ambient vibration analysis of an unstable mountain slope, *Geophysical Journal International*, **180**(2), 820–828.

Burjánek, J., Moore, J. R., Yugsi Molina, F. X., & Fäh, D., 2012. Instrumental evidence of normal mode rock slope vibration, *Geophysical Journal International*, **188**(2), 559–569.

Edwards, B., Michel, C., Poggi, V., & Fäh, D., 2013. Determination of Site Amplification from Regional Seismicity: Application to the Swiss National Seismic Networks, *Seismological Research Letters*, **84**(4), 611–621.

Fäh, D., Kind, F., & Giardini, D., 2001. A theoretical investigation of average H/V ratios, *Geophysical Journal International*, **145**(2), 535–549.

Fäh, D., Wathelet, M., Kristekova, M., Havenith, H.-B., Endrun, B., V., G. S., Poggi, Burjanek, J., & Cornou, C., 2009. Using ellipticity information for site characterisation using ellipticity information for site characterisation, *Technical report, NERIES JRA4*.

Hobiger, M., Bard, P.-Y., Cornou, C., & Le Bihan, N., 2009. Single station determination of Rayleigh wave ellipticity by using the random decrement technique (RayDec), *Geophysical Research Letters*, **36**(14), n/a–n/a, L14303.

Lontsi, A., Ohrnberger, M., & Krüger, F., 2016a. Shear wave velocity profile estimation by integrated analysis of active and passive seismic data from small aperture arrays, *Journal of Applied Geophysics*, **130**, 37 – 52.

Lontsi, A. M., Ohrnberger, M., Krüger, F., & Sánchez-Sesma, F. J., 2016b. Combining surface wave phase velocity dispersion curves and full microtremor horizontal-to-vertical spectral ratio for subsurface sedimentary site characterization, *Interpretation*, **4**(4).

Lontsi, A. M., García-Jerez, A., Molina-Villegas, J. C., Sánchez-Sesma, F. J., Molkenthin, C., Ohrnberger, M., Krüger, F., Wang, R., & Fäh, D., 2019. A generalized theory for full microtremor horizontal-to-vertical [H/V(z, f)] spectral ratio interpretation in offshore and onshore environments, *Geophysical Journal International*, **218**(2), 1276–1297.

Maranò, S., Reller, C., Loeliger, H.-A., & Fäh, D., 2012. Seismic waves estimation and wavefield decomposition: application to ambient vibrations, *Geophysical Journal International*, **191**(1), 175–188.

Poggi, V. & Fäh, D., 2010. Estimating rayleigh wave particle motion from three-component array analysis of ambient vibrations, *Geophysical Journal International*, **180**(1), 251–267.

Sambridge, M., 1999. Geophysical inversion with a neighbourhood algorithm—i. searching a parameter space, *Geophysical Journal International*, **138**(2), 479–494.

Wathelet, M., 2008. An improved neighborhood algorithm: Parameter conditions and dynamic scaling, *Geophysical Research Letters*, **35**(9).